Authors:

Robert W. Burroughs
ORCID: 0000-0003-4384-3430
Department of Ecology and Evolution
Stony Brook University, Stony Brook, NY.
Robert.Burroughs@stonybrook.edu

Christopher J. Percival
ORCID: 0000-0002-8883-9737
Department of Anthropology
Stony Brook University, Stony Brook, NY.
Christopher.Percival@stonybrook.edu

Natasha S. Vitek
ORCID: 0000-0003-0587-8907
Department of Ecology and Evolution
Stony Brook University, Stony Brook, NY.
Natasha.Vitek@stonybrook.edu

Data availability statement: All mapped and analyzed proteomics data and phenotypic data analyzed, along with R-scripts and ProteoRE workflow are included as Supplemental Materials. These Supplemental Materials will be made available publicly upon publication via Dryad Digital Repository DOI: 10.5061/dryad.kh18932j0. Raw proteomics data will be made publicly available on the MassIVE database with Dataset Identifier: MSV000098600.

Funding statement: Author RWB was funded via an Institutional Research and Academic Career Development Award (IRACDA) made to Stony Brook University from the National Institute of General Medical Sciences of the National Institutes of Health [K12GM102778], and startup funding to NSV from Stony Brook University.

Experiments were paid for via startup funding to NSV from Stony Brook University

Conflict of interest disclosure: Authors have no conflicts of interest.

Ethics approval statement: Live animal experiments were conducted in accordance with guidelines and regulations from Stony Brook University Institutional Animal Care and Use Committee (IACUC). Research was conducted in accordance with plan and procedures in approved protocol SBU IACUC 2023-0014.

Patient consent statement: Not Applicable.

Permission to reproduce material from other sources: Not Applicable.

Clinical trial registration: Not Applicable.

Reduced Dietary Protein Induces Changes in the Dental Proteome

Robert W. Burroughs[1,2], Christopher J. Percival[3], Natasha S. Vitek[1]

[1] Department of Ecology and Evolution, Stony Brook University, Stony Brook, NY, USA.

[2]Center for Inclusive Education, Stony Brook University, Stony Brook, NY, USA.

[3]Department of Anthropology, Stony Brook University, Stony Brook, NY, USA.

Abstract

Experimental studies have demonstrated that nutritional changes during development can result in phenotypic changes to mammalian cheek teeth. This developmental plasticity of tooth morphology is an example of phenotypic plasticity. Because tooth development occurs through complex interactions between manifold processes, there are many potential mechanisms which can contribute to a tooth's norm of reaction. Determining the identity of those mechanisms and the relative importance of each of them is one of the main challenges to understanding phenotypic plasticity. Quantitative proteomics combined with experimental studies allow for the identification of potential molecular contributors to a plastic response through quantification of expressed gene products. Here, we present the results of a quantitative proteomics analysis of mature upper first molars in *Mus musculus* from a controlled feeding experiment. Pregnant and nursing mothers were fed either a low-dietary protein (10%) treatment diet or control (20%) diet. Low-dietary protein was not associated with reduced molar size or skull length. However, expression of tooth-related proteins, immune system proteins, and actin-based myosin proteins were significantly altered in our low-dietary protein proteomics sample. The differential expression of immune proteins along with systematic reduction in actin-based myosin protein expression are novel discoveries for

tooth proteomics studies. We propose that studies that aim to elucidate specific mechanisms of molar phenotypic plasticity should prioritize investigations into the relationships between IGF regulation and tooth development and actin-based myosin expression and tooth development.

Research Highlights

A low-protein diet during development results in significantly altered protein expression for odontogenetic and osteogenic proteins, immune system proteins, and actin-based myosin proteins within *Mus musculus*, but does not alter skull length or molar size.

Introduction

Phenotypic plasticity, the differential expression of a phenotype, is often invoked as a way that organisms respond to changing environments. Within lab and common garden experiments, nutritional changes such as changes in the quantity of dietary protein induce plastic changes to mammalian cheek tooth phenotypes (Patton & Brylski, 1987; Paynter & Grainer, 1956; Shaw & Griffiths, 1963). Typically, these are changes in tooth size, size and shape of tooth cusps, and timing of eruption (Holloway et al., 1961; Patton & Brylski, 1987; Paynter & Grainer, 1956; Searle, 1954; Shaw & Griffiths, 1963). This demonstrates that there is plasticity in dental development that can provide a short-term, non-evolutionary response to changing environments (Levis & Pfennig, 2021). However, measures of plastic phenotypic response to environmental change often do not identify the molecular and genetic pathways underlying those changes. The use of quantitative proteomics to quantify differences in protein expression could allow for the

identification and study of pathways that are altered by an environmental change (e.g., are plastic). Here, we present a study characterizing protein expression variation in a sample of upper first molars (M1s) and phenotypic variation in lower first molars (lower M1s) from lab mice fed a low-protein diet as part of a controlled feeding experiment. This experiment was designed to induce developmental changes to dental traits and to identify proteins and associated pathways that may underlie phenotypic plasticity. This allows us to characterize those pathways most impacted by exposure to low dietary protein during embryonic and early postnatal tooth development.

Proteomics

Proteomics is broadly the field focused on identifying, annotating, and quantifying variation of proteins. Quantification of variation includes both protein sequence variation and protein expression variation. Informatics approaches are applied to protein spectral data collected via tandem liquid-chromatography mass-spectrometry (LC-MS/MS) (Heck & Neely, 2020). Protein expression profiles are typically tissue- and developmental stage-dependent and must be interpreted within the specific spatiotemporal contexts in which samples were collected (Rebeaud et al., 2021).

An assemblage of proteins that is expressed within a specific tissue or structure is often referred to as a ‘proteome’ (Sharma et al., 2020). For example, within the dental proteome enamel and dentin forming proteins are found in high abundance (Sharma et al., 2020). However, outside of dental tissues, these proteins are detected in low

abundance and only at certain developmental stages (Bansal et al., 2012; Ritchie, 2018).

If basic processes of tooth mineralization are impacted by dietary deficiency, we expect a change in associated protein expression and a change in phenotype such as occlusal pattern, size, and/or shape (Harjunmaa et al., 2014). It is possible that some aspects of tooth mineralization are more easily perturbed by environmental change than others and their associated pathways may more frequently underlie plastic changes. Measuring the tooth proteome may allow us to identify potential candidates underlying plastic changes in tooth phenotype.

Beyond stereotypical tooth-associated proteins, previous characterizations of the dental proteome have suggested that teeth serve as reservoirs of more general patterns of organismal protein expression during amelogenesis (tooth mineralization) (Froment et al., 2021; Giovani et al., 2021; Green et al.; Sharma et al., 2020). For example, Green et al. (2019) recovered immune system related proteins from enamel that was micro sampled from near the enamel-dentin junction of mineralizing pig molars. These immune proteins currently have no known function in amelogenesis. These proteins are definitively present within enamel tissue, but they may originate in nearby salivary glands that are in contact with enamel cell proliferation zones and regions of mineralization at the enamel-dentin junction (Green et al., 2019; Jagr et al., 2019). If mineralized teeth serve as an archive of broader organismal protein expression at the

time of mineralization, it is possible that tooth proteomic data could provide evidence of more generalized responses to environmental perturbations.

This Study

To determine what pathways are altered by an impoverished diet, we conducted a controlled feeding experiment and investigated protein expression in the cheek teeth. The study presented here is part of a larger research program that will also investigate the impacts of low dietary nutrition on a variety of tooth phenotypes. Pregnant and nursing mouse dams were fed a low protein or control protein diet and effects were measured in their offspring. Previous feeding studies on dietary protein quantity in rats and mice suggested that a threshold of 10-12% (by weight) dietary protein reduction from a control of 20-24% should induce phenotypically plastic changes to molar size, skull length, and disrupt timing of molar development (Barbeito-Andrés et al., 2016 2016; Holloway et al., 1961; Miller & German, 1999; Paynter & Grainer, 1956; Paynter & Grainer, 1961; Pucciarelli, 1980; Shaw & Griffiths, 1963).

With this context we anticipated that reduction in dietary protein would disrupt normal tooth development and alter protein expression patterns during embryonic and early postnatal development. We predicted a significant reduction in M1 size, consistent with previous reports (e.g., (Holloway et al., 1961; Paynter & Grainer, 1956; Paynter & Grainer, 1961; Shaw & Griffiths, 1963) and significant reduction in skull length based on previous studies in rat and mouse (e.g., (Barbeito-Andrés et al., 2016; Lobe et al., 2006; Miller & German, 1999; Pucciarelli, 1980). Previous studies suggested that halving

114 dietary protein would likely increase risk of infection and increase metabolic stress in
115 low protein mice (Giovani et al., 2021; Steward et al., 2023). Thus, we anticipated that
116 there might be additional proteomic signals related to stress or immune system function
117 if those protein signatures are preserved within dentition. Recovery of significant
118 differential expression of proteins because of a dietary change allowed us to identify
119 and rank the molecular pathways most likely to be perturbed by environmental
120 influences like dietary protein reduction.
121
122 **Methods**
123 **Data Availability**
124 All datasets, code, workflows, and raw phenotypic data reported are available as
125 Supplemental Materials on Dryad: Dryad DOI. Raw proteomics data are available on
126 MassIVE database by querying the following MassIVE identifier: MSV000098600.
127
128 **Feeding Experiment**
129 A breeding colony of inbred strain C57BL/6J (RRID: IMSR JAX:000664) mice was
130 established at the Division of Laboratory Animal Research at Stony Brook University, in
131 accordance with authorized IACUC protocol (SBU IACUC 2023-0014). Male and female
132 mice were acquired at 8 weeks of age and housed in residence to acclimate until
133 breeding began at 12 weeks of age. Males were placed with females for up to 72 hours
134 (3 day-night cycles) and females were checked daily for presence of a copulatory plug.
135 Once a plug was present or 72 hours had passed, the male and female were separated.
136 Females, regardless of plug presence, were then randomly assigned to control or

137 treatment diets to ensure that any developing embryos were on as consistent a diet as
138 possible. Mice assigned to the control group were fed a 20% raw protein diet (PicoLab
139 Rodent Diet 20, 5053). Mice assigned to treatment were fed a 10% raw protein diet
140 (Mod LabDiet 5053 with ~10% Protein Red, 5BQM). Prior to this assignment, all
141 specimens consumed the control diet.
142
143 If females were not pregnant, as evidenced by swollen abdomen after ~7 days post-
144 mating attempt, low-protein females were cycled back to the control protein (20%) diet.
145 They were re-acclimated to that diet for 14 days before additional mating was
146 attempted. To ensure that additional stress was not induced via single housing, pairs of
147 females were housed together during acclimation and pregnancy. Mating timings were
148 staggered to ensure that two females in the same cage would not give birth at the same
149 time. This allowed for the separation of females and their litters once they had given
150 birth.
151
152 Pregnant and nursing females in the treatment group were fed only the low-protein diet
153 for the remainder of their lifespan. Offspring were weaned at approximately ~21 days
154 postnatal (P21). Siblings were housed with their respective sex and fed their respective
155 diets until P28 to ensure full eruption of the third molars. Dams and offspring were
156 euthanized when the offspring were P28. Dams were not reused to avoid introducing
157 bias related to improvement of maternal care from first to second litter (Weber & Olsson,
158 2008). A total of 12 litters (7 treatment, 5 control) constituting 74 offspring (treatment
159 n=34, control n=30) from this feeding experiment were collected. Aside from the 74

160 collected offspring, there was postnatal attrition of one full litter of treatment pups (n=8),
161 where the mother declined to nurse the pups. The smallest pup from each of five litters
162 (treatment n=3; control n=2) also did not survive to weaning.
163
164 **Sampling**
165 For proteomics data we opportunistically sampled specimens from four litters of our
166 feeding experiment. In our sample, males were the more common sex, and thus we
167 selected by random, four male sibling pairs for destructive sampling. Selecting only
168 males also removed variation in protein expression that would be associated with
169 specimen sex within our small sample. The upper first molar (upper M1) was selected
170 for protein extraction because of its ease of extraction and because it and its lower jaw
171 counterpart are the first molars to develop and erupt (Figure 1A). Eight upper M1s
172 (treatment n=4; control n=4) were extracted from sibling pairs from four litters
173 immediately after euthanasia by dissecting away the maxillary gingiva and exposed
174 maxillary bone to reveal tooth roots. A blunt probe was used to lever the tooth out.
175 Excess tissue, including any root bundle, was removed with forceps. Extracted teeth
176 were then washed with 70% ETOH, wiped dry with a clean Kimwipe, and stored in new
177 cryotubes. Teeth were placed into a -80ºC freezer and maintained at -80ºC until
178 preparation for protein quantification.
179
180 For phenotypic data, we sampled the left lower first molar (lower M1) of specimens from
181 four treatment and four control litters. These litters include the four litters sampled for
182 proteomics. We measured the phenotype of 50 (treatment n=24; control n=26), where

24 were males and 26 were females. Three of the specimens sampled for proteomics (2 controls, 1 treatment) were excluded from the phenotypic data because they were held out for future synchrotron scanning. Specimen data are included in Supplemental Materials.

Phenotyping

We utilized µCT imaging to generate high-fidelity 3D surfaces of mouse specimens. This approach allows us to utilize semi-automated phenotyping approaches. We batch scanned specimens at the New York Institute of Technology Visualization Center on a Bruker Skyscan 1173 at 75kV, 106µA, at a resolution of 19.938µm. Specimens were decapitated post-euthanasia and ethafoam was inserted to separate the upper and lower dentition. Heads were then wrapped in Kimwipes and stacked vertically in 50ml Falcon tubes, with males and females grouped separately within the tube and one to two litters of the same type (e.g., all control or all treatment) per tube. Litters were separated by stacked ethafoam discs that form a visual barrier in reconstructed scan data.

Post-processing of µCT data was done at Stony Brook University, by author RWB, utilizing 3D Slicer (Fedorov et al., 2012). Reconstructed batch scans were loaded into Slicer and individual specimens were cropped from the batch scan volume. Minimum thresholding was used to segment all bony elements within the scan. The Islands segmentation tool was used to separate out the largest element within the segment, the cranium. Once segmented, crania were converted to 3D models. It was necessary to

segment the entire tooth row, as opposed to isolate the lower M1, due to contact between teeth. Minimum thresholding was again applied, but with increased minima compared to bony elements to isolate the denser enamel. The Scissors tool was used to circle the lower left tooth row and “Erase Outside” was selected to remove all remaining elements within the segment. Finally, the Islands tool was again used to keep only the largest element within the segment (the tooth row). Once segmented, toothrows were converted to 3D models.

We utilized landmarks to measure phenotypic data on 3D models. To place landmarks, we utilized Automated Landmarking through Point cloud Alignment and Correspondence Analysis (ALPACA) implemented within the 3D Slicer SlicerMorph extension (Porto et al., 2021; Rolfe et al., 2021). The strength of ALPACA lies in rapid implementation and reduced user bias in landmark placement for landmark projection. ALPACA accomplishes this with a point cloud-based deformation of a reference landmark template and mesh to match non-reference specimens. Once the deformation has occurred, landmarks from the reference specimen are projected onto the non-reference specimen. Because this method utilizes a deformation-based approach it is necessary that specimens be similar in shape (as they are in this intraspecific study of a single tooth) and that placed landmarks be quality checked after running ALPACA. We generated two reference templates: 1) a control cranium with two landmarks for calculating straight-line skull length, 2) a control lower M1 with 25 landmarks representing tooth outline/crown footprint (Figures 1B and 1C). After ALPACA was run,

228 a single author (RWB) checked all of ALPACAs landmark position predictions and
229 moved any landmarks that were not properly projected.
230
231 Analysis of landmark data was conducted in **R** with core R tools (RCoreTeam, 2023),
232 the **geomorph** (Adams et al., 2013) package, with visualization via the core **plot**
233 functions and **ggplot** package (Wickham, 2016). The landmark files and R script are in
234 Supplemental Materials. To test hypotheses of changes in skull-length we measured the
235 line between landmarks at the apex of the foramen magnum and the junction between
236 the maxillae (Figure 1B). A Welch's T-Test was calculated using the **t.test** function in R
237 to determine if there was a significant difference between treatment and control group
238 mean skull lengths. Because our prediction was that treatment specimens would be
239 smaller, we utilized a single-tail alternative hypothesis, implemented in R as "greater
240 than".
241
242 Crown footprint area of the left lower first molar (lower M1) was represented by 25
243 landmarks placed around the widest portion of the crown (Figure 1C). These landmarks
244 were used to estimate a convex hull that approximates the tooth crown area. We
245 compared mean crown area estimates between groups using Welch's T-Test, as
246 described for skull length.
247
248 The decision to phenotype the lower M1 while quantifying the proteome of upper M1
249 was based on sampling constraints. Both molars develop simultaneously, rendering
250 them as comparable as possible, while simultaneously accounting for the potential

251 reciprocal destructive sampling of each method collection approach. Previous studies
252 indicate that high power µCT has been shown to damage DNA and could possibly
253 degrade proteins (Immel et al., 2016) and our proteomics protocol required destroying
254 the entire upper M1. Choosing the lower molar for phenotyping also aids in future
255 phenotypic comparisons because lower molars are usually found in higher abundance
256 within paleontological samples, resulting in studies of phenotypic evolution and plasticity
257 often emphasizing measures of lower molars (Bell & Jass, 2011; Burroughs, 2019;
258 Procopio et al., 2018; Ungar, 2010). We chose an outline-based approach over
259 traditional straight-line measurements because crown area has been shown to be a
260 more sensitive tool for assessing size (Hopkins, 2018).
261
262 **Protein analysis by LC-MS/MS**
263 For protein analysis we first determined if our extraction and proposed sampling worked
264 by initially sampling only two treatment and two control specimens. After validating our
265 protocols, we sampled the remaining two treatment and two control specimens. Proteins
266 were isolated in 5% SDS, 100mM TEAB, 10mM DTT using a Precellys bead
267 homogenizer for two cycles and spun at 16,000 x G for 5 minutes, which pulverized the
268 tooth tissue. Supernatants were reduced at 55ºC for 30 minutes, and cysteines were
269 alkylated with 25mM iodoacetamide for 30 minutes at room temperature in the
270 dark. Samples were acidified with phosphoric acid, proteins were then precipitated with
271 90% methanol, 50mM TEAB, and bound to S-Trap solid phase cartridges (Zougman et
272 al., 2020). Protein precipitates were washed with 90% methanol, 50mM TEAB and
273 digested with trypsin (20µg, Sigma-Aldrich. Trypsin, TPCK-treated; #4352157) at 47ºC

274 for two hours. We ran two blank STRAP samples per analytical sample, no protein or
275 peptide was recovered from blank STRAP samples, except for a single keratin peptide
276 at m/z 1082. Precipitates were then sequentially eluted with 50mM TEAB, 0.2% formic
277 acid, and 50% acetonitrile, the 0.2% formic acid elution step was by centrifugation at
278 4000 x G for 1 minute each. Peptides were dried by vacuum centrifugation, desalted
279 using HLB SPE cartridges (Waters), dried and resuspended in 20µl 0.1% formic
280 acid/water.
281
282 Peptides were analyzed by C18 reverse phase LC-MS/MS (Thermo Nano1200) using a
283 2µl injection volume. HPLC C18 columns were prepared using a P-2000 CO2 laser
284 puller (Sutter Instruments) and silica tubing (100µm ID x 15 cm) and were self-packed
285 with 3u Reprosil resin. Peptides were separated using a flow rate of 300 nl/minute, and
286 a gradient elution step changing from 0.1% formic acid to 40% acetonitrile (CAN) over
287 90 minutes, followed by a 90% CAN wash and re-equilibration steps (buffer A 0.1%
288 formic acid/water, buffer B 90% acetonitrile/water with 0.1% formic acid). Parent peptide
289 mass and collision-induced fragment mass information were collected using an orbital
290 trap (Q-Exactive HF; Thermo) instrument followed by protein database searching using
291 Proteome Discoverer 2.4 (Thermo). Electrospray ionization was achieved using spray
292 voltage of ~2.3 kV. Information-dependent MS and MS/MS acquisitions were made
293 using a 50ms survey scan (m/z 375 – 1400) at 60,000 resolution, followed by ‘top 20’
294 consecutive second product ion scans at 15,000 resolution. Peptide and spectra false
295 discovery rates were set to 0.01 and 0.05 FDR bins, with 10ppm MS and 0.05Da MS2
296 tolerances, allowing up to 2 missed tryptic cleavages, and a minimum peptide size of 6

297 amino acids. Variable modifications included M-oxidation, NQ-deamination, and ST
298 dehydration. Peptide-specific label free quantitation (mapping) was performed using
299 Proteome Discoverer 2.4 (SequestHT Percolator algorithm), linking peptides to
300 annotated mouse proteome (Uniprot mouse 16982 sequences; 4-2019, downloaded
301 October of 2023) and the MQ contaminant dataset for standardized protein
302 identification. Label free abundance estimations were performed (Sequest HT LFQ).
303 Raw data files are available on the MassIVE database using identifier MSV000098600.
304
305 **Filtering**
306 To assess if dietary changes resulted in significantly altered protein expression, we first
307 filtered our mapped proteomic data. Filtering was done in ProteoRE (Mehta et al.,
308 2023). Because spectral ionization can vary between LC-MS/MS analyses (e.g., (Muntel
309 et al., 2015; Z. Wang et al., 2024)) we initially treated our dataset as two distinct
310 datasets, representing the initial sampling (Group 1) and additional sampling (Group 2)
311 (Supplemental Materials). There was no expectation that Groups 1 and 2 were
312 substantially different from one another based on the experimental procedure: groups
313 differed only by the date of LC-MS/MS analysis. We chose a conservative approach of
314 filtering each dataset individually and concatenating the resulting filtered datasets,
315 ensuring that only proteins represented in both datasets were used for downstream
316 analyses and interpretations. Each sample group was initially filtered by excluding all
317 mapped proteins that had any one of the following criteria: A minimum false discovery
318 rate (q-value) greater than 0.05, representation by fewer than two peptides, or three or

fewer peptide spectral matches (PSMs). These criteria were selected based on proteomics field standard practices (Al-Amrani et al., 2021).

Mapped Proteomics Analysis

To concatenate our results, a Venn analysis was performed to find the set of proteins identified as unambiguously present in both groups, resulting in a combined group (CG) dataset. This dataset reflected the shared mapped proteins between all eight (four control, four treatment) specimens in our sample. Groups 1 and 2 were further filtered to identify proteins with significant changes in protein expression between treatment and control specimens. First, proteins where at least one treatment specimen in each group had an abundance ratio adjusted p-value ≤0.05 were retained (n=135). Then, proteins that had missing data for two or more specimen comparisons were discarded (n=15). Those two datasets were subsequently concatenated via a Venn analysis to form a combined group significant (CGSig) dataset. The result is that every protein in CGSig is significantly differentially expressed in at least one treatment/control comparison in Group 1 and at least one treatment/control comparison in Group 2.

Here, the abundance ratio is a normalized ratio of estimated protein abundance, based on peak intensity, for one proteomics sample over another proteomics sample, in our case a treatment specimen over a control specimen. Because protein abundances can vary significantly in terms of magnitude between samples in label free quantification, the estimated protein abundances are commonly transformed on a Log2 scale to normalize (adjust) them (Liu & Zhang, 2021). To calculate the p-value for adjusted abundance

342 ratios p-values we used a two-tailed Students' T-Test. One result of this transformation
343 is that some calculated abundance ratios will effectively become -∞ or ∞ but are
344 represented in the dataset as values of -3.32 or 3.32. We calculated the average Log2
345 fold change reported in Table 1 by taking the mean of the estimated abundance ratios
346 from samples that had significant p-values, excluding significant samples that were
347 equal to -3.32 or 3.32. For some samples, calculated means were close to 0 and/or
348 removal of one outlier could change the sign (and thus interpretation) of the mean. In
349 those cases, we do not provide an average value, instead we provided the number of
350 specimens and their direction of fold change (Up/Down) (Table 1).
351
352 To identify protein functions, associated interactions, and general biological profiles
353 represented in CG and CGSig we performed Gene Ontology (GO) enrichment analysis
354 via the ClusterProfiler tool of ProteoRE and Pathway Enrichment Analysis via
355 REACTOME (Croft et al., 2011; Wu et al., 2021). For GO enrichment analyses, we
356 queried at two ontology levels, using cutoffs for p-value of 0.05 and q-value of 0.05.
357 Outputs for GO analyses were used to assign broad categorical function to proteins
358 (Table 1) based on Metabolic Functions, Cellular Component, and Biological Processes
359 categories (Figure 3).
360
361 For pathway enrichment analysis via REACTOME we queried the *Mus musculus*
362 REACTOME for the proteins found in the CGSig dataset. To calculate enrichment, the
363 number of entities (in our case proteins) identified as belonging within a specific
364 pathway are identified. Then the total number of entities (proteins) that could be

365 contained in that pathway is calculated and divided by the total number of entities
366 (proteins) from the organism (in our case *Mus*). The resulting 'Entity Ratio' is used to
367 correct for pathway size to determine which pathways are overrepresented compared to
368 a random distribution. A pathway is considered 'enriched' when the input from the
369 dataset (x) is a higher proportion of the total number of entities (n) than would be
370 expected by chance. The resulting probability estimate is represented by a p-value
371 calculated on a 95% confidence interval and pathways with Entities p-value ≤ 0.05 are
372 significantly enriched. Enriched pathways were then ranked based on the Entity Ratio,
373 which represents the percentage of all *Mus* proteins in that pathway with a significant
374 enrichment in our analysis (i.e., an Entity Ratio of 0.04 represents 4% of all *Mus*
375 proteins known in that pathway). Pathways with higher entity ratios are ranked higher
376 within Table 2.
377
378 **Preliminary Test of Developmental Archive**
379 Prior research and the design of our study allowed us to conduct a preliminary
380 investigation of whether enamel and dentin proteomes represent an archive of protein
381 expression during mineralization, rather than proteins expressed earlier in tooth
382 development or at the time of specimen collection. We queried the Mouse Gene
383 eXpression Database (GXD) to determine if a subset of proteins was expressed at
384 developmental stages prior to the onset of mineralization, during mineralization, or after
385 mineralization was complete. First, we investigated proteins known to be expressed
386 during tooth mineralization (Pandya et al., 2017). The study of Pandya et al. (2017)
387 reported 24 proteins present during tooth mineralization, we identified 20 of those 24

388 proteins in our CG dataset. We also investigated proteins related to
389 odontogenesis/osteogenesis, immune, and actin-based myosins from our CGSig
390 dataset. A protein's associated gene being expressed during mineralization, but not
391 earlier or later in time, would support the argument that tooth proteomes represent a
392 specific window of development during amelogenesis. The table containing the proteins
393 queried in the GXD is within Supplemental Materials.
394
395 **Results**
396 **Phenotyping**
397 We found no significant differences in size between treatment and control groups
398 (Table 3). Mean skull length for the treatment group was 19.20mm and control group
399 was 19.03mm (Figure 2A). Mean crown area for treatment group was 1.03mm^2 and
400 control group mean was 1.02mm^2 (Figure 2B).
401
402 **Proteomics**
403 Within G1, a total of 2189 unique proteins were mapped (Supplemental Materials). 1622
404 unique proteins were mapped for G2 (Supplemental Materials). The combined group
405 (CG) of proteins shared between G1 and G2 was 1469 unique proteins (Supplemental
406 Materials). Of the combined group, there were a total of 120 proteins with significant
407 differential expression (fold change) (CGSig; Table 1; Figure 4; Supplemental Materials
408 Figures 1-6).
409

410 Gene ontology profiling revealed that both CG and CGSig are comprised of sets of
411 proteins primarily associated with the Binding (in Molecular Function), the Cell generally
412 (as opposed to a specific cellular component), and the Biological Process of Metabolism
413 (Figure 3; Supplemental Materials). Pathway enrichment analysis via REACTOME
414 identified 387 biological pathways associated with significantly differentially expressed
415 proteins (Supplemental Materials). Of those 387, 34 were significantly enriched ($p \leq$
416 0.05) (Table 2). Approximately 47% of matched proteins are represented in the top 6
417 enriched pathways (Entity Ratio ≥ 0.01) (Table 2; Supplemental Materials).
418
419 **Odontogenesis and Osteogenesis Proteins**
420 A total of 8 proteins in CG were identified as belonging to biomineralization seven
421 proteins associated of them had significant differential expression (Log2 fold change)
422 between treatment and control groups (Table 1; Figure 4). In low-protein treatments, the
423 major enamel-forming protein, Amelogenin X (AMELX) had an average -1.52-fold
424 change in expression. One of the two major dentin-forming proteins, Dentin
425 sialophosphoprotein (DSPP) had a 1.77-fold increase in expression. The other dentin-
426 forming protein, Dentin matrix acidic phosphoprotein 1 (DMP1) did not have a clear
427 direction of differential expression; three treatment comparisons showed an increase in
428 protein expression, while two had a decrease in expression. For osteogenesis, Integrin
429 alpha-V (ITGAV) had -2.66-fold change and Tartrate-resistant acid phosphatase type 5
430 (ACP5) had -1.71-fold change. The remaining two osteogenic proteins Collagen alpha-
431 1(II) chain (COL2A1) and Galectin-7 (LGALS7) had variation that made interpretation

432 unclear. For COL2A1, one specimen had increased and two had decreased expression.
433 For LGALS7, three were increased and two decreased.
434
435 **Inflammation and Immune Response**
436 A total of 229 proteins were associated with Immune System Response. Nine proteins
437 associated with inflammation and immune system response had significant differential
438 expression (Log2 fold change) between treatment and control groups (Table 1; Figure
439 4). Two of the nine proteins, S100-A8 (S100A8) and Coagulation factor X (F10), had a -
440 1.27 and -0.23 fold change in treatment groups, respectively. Five of the nine proteins
441 had increases in expression: 0.92 for Platelet factor 4 (PF4), 1.10 for Galectin-3
442 (LGALS3), 1.50 for BPI fold-containing family A member 2 (BPIFA2), 2.30 for Protein
443 AMBP (AMBP), and 2.40 for Arginase-1 (ARG1). Two of the immune proteins,
444 Apoptosis-associated speck-like protein containing a CARD (PYCARD) and
445 Calmodulin-4 (CALM4), lacked consistent signal between pairwise specimen
446 comparisons. For PYCARD, one specimen showed increased expression and one
447 showed decreased expression. For CALM4, two specimens were increased in
448 expression and one decreased in expression.
449
450 **Muscle Contraction**
451 A total of 42 proteins were associated with muscle contraction 13 of those proteins had
452 significant differential expression. All of them had decreased expression for treatment
453 specimens (Table 1; Figure 4). Seven of the 13 proteins are actin-based myosins
454 (Myosins 1, 4, 7B, 8, Myosin Light chain 1, Tropomyosin 2, and Myosin regulatory light

455 chain 2), with the remaining six being actin-specific proteins (Troponin T, Actins Alpha 1
456 and Alpha 2, Titin, and Four and a half LIM domains protein 1).
457
458 **Preliminary Test of Developmental Archive**
459 Genes associated with two of 20 tooth proteins previously found during mineralization
460 (Pandya et al., 2017) are also found in tooth tissues prior to the onset of amelogenesis
461 based on a query of GXD. Those genes are *Alpl* and *Itgb1*. Both are found only in the
462 tooth developmental stage immediately prior to amelogenesis (TS21 associated with
463 embryonic days 12.5-14). The genes associated with the remaining 18 proteins are
464 found only in developmental stages associated with molar amelogenesis (TS22+,
465 embryonic day 15 through postnatal day 8). Querying genes associated with our
466 proteomic sample's differentially expressed immune and actin-based myosin proteins
467 within GXD revealed that immune genes are universally expressed within tooth tissues
468 during all reported stages until adulthood. Actin-based myosins were present from the
469 onset of mineralization forward. Two of the actin-based myosins (*Actn2* & *Fhl1*) were
470 reported as definitively absent from tooth tissues at E14.5 (i.e., just prior to
471 mineralization) (Visel et al., 2004). Additionally, one gene (*Myh1*) was present in
472 mineralization stages but was definitively absent from postnatal week 6-8 aged mouse
473 specimens (Freeman et al., 1998).
474
475 **Discussion**
476 **Phenotyping**

Our hypotheses were that specimens in the treatment group would have reduced skull length and M1 size, results we did not recover. Both phenotypic results were unexpected because many studies have reported variation in skull size associated with nutritional quality in rats, mice, and pigs (e.g., (Barbeito-Andrés et al., 2016; Dickerson & Hughes, 1972; Lobe et al., 2006; McCance et al., 1961; Miller & German, 1999; Pucciarelli, 1980, 1981), and four previous studies reported variation in the size of the M1 due to dietary changes (Paynter & Grainger, 1956; Holloway et al., 1961; Paynter & Grainger, 1961; Shaw & Griffiths, 1963). Why then did we not recover similar signals?

First, we note that these previous studies sampled specimens at different ontogenetic stages than we did, most sampled specimens that were older than ours (40-days postnatal to 10-months postnatal), a single study (Barbeito-Andrés et al. 2016) sampled specimens younger than ours (embryonic day 18 to postnatal day 1). Considering skull length, mice grow continuously until they reach sexual maturity and rapidly between birth and weaning. It is possible that any differences in skull length were simply not manifested at the ontogenetic stage we sampled. This does not explain, however, the lack of difference in M1 size reported previously, because M1s are determinate in growth and cease to grow by postnatal day 8 (Ungar, 2010; Pandya et al, 2017). In comparison to our study design using 10% dietary protein as the low-protein treatment, some other studies used dietary protein quantity as low as 8% (e.g., Paynter & Grainger, 1956; Holloway et al., 1961; Paynter & Grainger, 1961; Shaw & Griffiths, 1963; Miller & German 1999). This small additional reduction in dietary protein may be sufficient to trigger effects. Finally, we recognize that different dental and cranial traits

are impacted by dietary protein more readily than others. Cranial traits have been reported to be less impacted by reduced dietary protein than postcranial traits (e.g., McCance et al. 1961; Lobe et al. 2006) and M1 size may be less impacted than other traits of the M1 (e.g., angle of cusps) (Paynter & Grainger, 1956; Holloway et al., 1961; Paynter & Grainger, 1961).

At present we can only conclude that there is no difference in M1 size or skull length of specimens from our groups. However, our proteomic results (discussed in detail below) inform us that development of the tooth was perturbed in ways that likely impact other aspects of tooth phenotype. For instance, changes in relative enamel or dentin thickness would not be recovered by our estimates of size, because these are internal structural changes to tooth composition. Future more comprehensive phenotyping efforts may reveal significant differences.

Developmental Archive

Results from GXD queries support the argument that our tooth proteome dataset primarily represents gene expression during mineralization and not prior to mineralization. For example, genes for actin-based myosins of interest within our dataset are not expressed in mouse teeth prior to the onset of amelogenesis. While it is not possible to say whether the measured immune-system proteins in our proteomic sample were expressed during mineralization or at the time of euthanasia, previous studies (e.g., Green et al., 2019; Jagr et al., 2019) have identified immune and inflammation related proteins incorporated in tooth tissues, either within enamel itself or

523 within other tissues of the enamel-dentin junction, such as salivary glands. In our case,
524 we recover several of the immune related proteins reported by those studies, including
525 S100A8 and CALM4, potentially supporting the idea that molar enamel represents an
526 archive of gene and protein expression during amelogenesis. This conclusion is further
527 supported by the fact that the gene for differentially expressed MYH1 in our dataset is
528 not expressed after mineralization, indicating our MYH1 signal likely represents protein
529 expression during mineralization rather than a later time point (Freeman et al. 1998).
530 Further, we would not expect expression of amelogenesis-specific genes or proteins
531 after the end of mineralization, because of the cessation of proliferation of ameloblasts
532 and lack of vascularization within the fully mineralized tooth (Alghadeer et al., 2023;
533 Nanci, 2007). While this hypothesis requires further directed experimental validation,
534 our results support the concept that the recovered tooth proteome represents a limited
535 window of development.
536
537 **Odontogenic Proteins**
538 We predicted that proteins associated with enamel and dentin formation would be
539 altered by our feeding experiment, and specifically that they would be decreased in
540 expression. The major enamel forming protein, AMELX, was significantly reduced in
541 expression for treatment specimens (Table 1; Figure 4). We anticipated that our dietary
542 protein reduction would result in decreased tooth size, associated with decreased
543 AMELX expression, because AMELX is a necessary component for the formation of
544 enamel. While changes in AMELX met our expectations, measures dentin forming
545 protein expression and lower M1 size did not.

546

547 In the case of DMP1, there is not a clear signal to interpret whether expression was
548 increased or decreased in our proteomics sample. This highlights the challenges of
549 drawing interpretations from proteomic data where individual variation can influence the
550 overall interpretation. This challenge is recognized by the field of quantitative
551 proteomics, but still represents an area where increased research efforts will be needed
552 (Al-Amrani et al., 2021; Chantada-Vazquez et al., 2022; Liu & Zhang, 2021; Steward et
553 al., 2023). A clearer interpretation of DMP1 expression, would be helpful for constructing
554 future hypotheses. For instance, decreased expression of DMP1 should lead to
555 decreased expression of DSPP and dentin hypomineralization, suggesting that DMP1
556 and DSPP expression contribute significantly to dentinogenesis imperfecta (Orsini et al.,
557 2014; Shi et al., 2020). Being able to robustly identify such patterns or, at minimum,
558 make supported interpretations based on the variable evidence, will enhance the utility
559 of future quantitative proteomic studies.

560

561 Our finding of increased DSPP expression seemed initially counterintuitive. However,
562 this result is supported by a recent study of protein expression in a hypomineralized
563 enamel defect found in humans (Mukhtar et al., 2022). In this study of hypomineralized
564 molars, the enamel defect impacts the first permanent molars of children and results in
565 a significant reduction in mineral density from normal teeth (Mukhtar et al., 2022). This
566 reduced density was associated with downregulation of AMELX, upregulation of DSPP,
567 but no reported differences in DMP1 expression (Mukhtar et al., 2022).

568

569 The causal mechanism for the pattern of increased DSPP expression is unknown. The
570 general role of DSPP is to control the conversion of dental pulp cells into odontoblasts
571 via binding with Integrin beta 6 (ITGB6) (Ritchie, 2018; Wan et al., 2016). Previous work
572 indicated that mice with either a DSPP heterozygous ($DSPP^{+/-}$) or DSPP knockout
573 ($DSPP^{-/-}$) genotypes experience dentin dysplasia and dentinogenesis imperfecta due to
574 haploinsufficiency of DSPP (Shi et al., 2020). Haploinsufficiency suggests that dentin is
575 impacted when DSPP expression is decreased but does not indicate what phenotype
576 results from elevated DSPP expression. Amelogenesis imperfecta enamel is typically
577 thin and chalky while dentin appears to be normally mineralized, suggesting that DSPP
578 overexpression does not result in dentin hypermineralization, but this has not been
579 experimentally validated and dentin structure was not reported by Mukhtar et al. (2022).
580
581 Our proteomic results appear consistent with protein expression patterns associated
582 with amelogenesis imperfecta and not dentinogenesis imperfecta, based on the shared
583 expression changes for AMELX and DSPP (Mukhtar et al., 2022; Orsini et al., 2014; Shi
584 et al., 2020). It is unlikely that both amelogenesis and dentinogenesis imperfecta are
585 simultaneously present within a single specimen's dentition. Only a single study has
586 reported compounded presence of amelogenesis and dentinogenesis imperfecta, which
587 occurred in an MSX2 knockout transgenic line (Aioub et al., 2007).
588
589 It is possible that the signal here is due to experimental design of this study, where
590 enamel and dentin are pooled together. The concern is that dentin constitutes a larger
591 amount of the overall tooth and could 'swamp' the proteomic signal. However, this

592 appears unlikely due to consistent signals of expression changes for many proteins not
593 related to dentin. In cases where a set of proteins ‘swamp’ the signal, it is due to
594 exceptionally high abundance of certain proteins, e.g., raw blood is dominated by ~20
595 proteins related to hemoglobin, swamping out other protein signals (Molloy et al., 2023).
596 In our case, recovery of 1469 proteins and 120 significantly different proteins associated
597 with numerous processes suggests that our signal is not driven by one tissue or
598 category of proteins within the pooled tissue sample.
599
600 Thus, we conclude that our measures of differentially expressed amelogenesis-
601 associated proteins indicate that the development of thinner and less mineralized dental
602 enamel could be a phenotypically plastic response to reduced dietary protein during
603 early development. Such a result would help explain why there are disparate signals
604 between proteomic and phenotypic results: while tooth size is not affected, tooth or
605 microstruture composition may be. To test this hypothesis, it is necessary to utilize
606 synchrotron scanning or destructive sampling in the form of histology. For now, it
607 remains to be tested if the mouse molars from our study have amelogenesis imperfecta.
608
609 **Immune and Inflammation Proteins**
610 Previous work on mapping protein expression across micro-sampled enamel sections
611 of pig molars had suggested that there was possibility of recovering immune and
612 inflammation related proteins from mineralized dentition (Green et al., 2019). In their
613 case, Green et al. (2019) were constructing a detailed map of proteomic expression
614 associated with amelogenesis. Their reported immune system proteins were localized

615 from enamel which came from along the enamel-dentin junction (Green et al., 2019).
616 Their study was not designed nor attempted to induce differential protein expression
617 based on experimental procedures. In our case, we were unsure if we would recover
618 immune and inflammation proteins because we created a tissue-averaged signal by
619 crushing and processing the entire M1. By finding these proteins in our proteomics
620 sample and recovering differential expression of them, we present a novel result of
621 immune response to an environmental change. Of the nine immune or inflammation
622 response proteins with significant fold change, five were increased in expression for
623 treatments relative to controls, two were reduced in expression, and two had mixed
624 interpretations (Table 1).
625
626 Seven of the nine proteins are primarily associated with neutrophil degranulation,
627 including transport and proliferation of neutrophils. Of these seven, five were increased
628 in expression. However, Calmodulin 4 (CALM4) had a mixed interpretation and
629 coagulation factor X (F10) was reduced in expression. Neutrophils function as critical,
630 but specialized, immune system response cells. Neutrophils contain granules of multiple
631 types (azurophilic, specific, ficolin-rich, tertiary, and secretory), that target specific
632 threats and/or regulate immune system response to specific infectious threats
633 (Eichelberger & Goldman, 2020; Othman et al., 2022 ; Yin & Heit, 2018).
634
635 The precise nature of what was being targeted by immune system activation is
636 unknown. However, the result of F10 being reduced in expression may provide some
637 insight into the potential infectious threat. Deficiency of F10 has been implicated as part

638 of an immune response to the common, antibiotic-resistant, bacterium *Acinetobacter*
639 *baumannii* (Choby et al., 2019). In those cases, F10 deficiency is indicative of an
640 increased abundance of neutrophils and macrophages (Choby et al., 2019). Thus,
641 though F10 is decreased in expression, relative to the increase in five other neutrophil
642 degranulation proteins, the combination of patterns supports a conclusion that our
643 treatment group had higher immune system response than our control group. Future
644 research efforts to systematically compare immune-related proteomic signatures from
645 mineralized structures to standardized health monitoring tools could prove fruitful.
646
647 We also recovered changes in PYCARD and S100A8 within our proteomics sample,
648 that are indicative of an inflammation response (Table 1). Studies have indicated that
649 PYCARD directly mitigates inflammation when upregulated and contributes to
650 inflammation when downregulated (Sartoretto et al., 2019; Wittmann et al., 2021). In our
651 sample, one treatment specimen showed a moderate increase in PYCARD expression
652 over controls, and one showed a moderate decrease (Table 1). Importantly, deviation in
653 either direction suggests that there is either an increased response to inflammation
654 (increased expression) or increased inflammation present (decreased expression)
655 (Sartoretto et al., 2019; Wittmann et al., 2021). Reduced expression is recovered for
656 S100A8, consistent with an ongoing physiological response to inflammation (S. Wang et
657 al., 2018). These patterns of differential expression may represent increased
658 inflammation response in some of the treatment specimens, as compared to control
659 specimens. Due to the limited nature of our data and potential variation in inflammation
660 response between specimens, these results should be interpreted cautiously.

661

662 Because of our controlled experimental design, we postulate that reduced dietary
663 protein is the cause of increased inflammation. A recent study investigating the impact
664 of low dietary protein during gestation indicates that intrauterine inflammation can occur
665 and result in increased inflammation present in the offspring of Syrian golden hamsters
666 (Mohammed et al., 2023). While Mohammed et al. (2023) focused on measuring
667 inflammation of the liver of the offspring, the connection between low dietary protein
668 during embryonic and postnatal development and increased inflammation was strongly
669 established. Our study and results further support this connection. Future studies should
670 aim to systematically investigate proteomic signals of mineralized structures along with
671 standardized inflammation panels. This would further establish the connection between
672 dietary protein, inflammation, and the signals archived within mineralized structures.
673

674 **Muscle Contraction Proteins**

675 All thirteen significantly modified Muscle Contraction pathway proteins were reduced in
676 expression. They were predominantly actin-based myosins, which play a critical role in
677 cellular movement and structure formation by acting as motor molecules (Guhathakurta
678 et al., 2018). Actin-based myosins are broadly implicated in the proper development of
679 many tissues, including dentition (Du et al., 2024; Guhathakurta et al., 2018; Luis &
680 Schnorrer, 2021). During dental development actin-based myosins contribute to the
681 proper formation of enamel rods by transporting ameloblasts (Duverger & Morasso,
682 2018). Lower expression of actin-based myosins, including some of those that are
683 differentially expressed in our study (e.g., Myosin-1, Myosin-4, Myosin-8, and Tropinin 1)

684 are associated with the syndromic form of amelogenesis imperfecta (Duverger &
685 Morasso, 2018). To date, no proteomic study of dentition has recovered differential
686 expression of actin-based myosins, but none of the previous dental proteomic studies
687 attempted to experimentally induce differential expression of these proteins. Future
688 investigations should center on understanding the distribution of actin-based myosins
689 within the tooth and the correlation between protein expression in teeth and other
690 tissues when dietary-protein is reduced.
691
692 **Potential Pathways for Phenotypic Plasticity**
693 We recovered 34 significantly enriched REACTOME pathways from our 120 significantly
694 differentially expressed proteins. Among those pathways, two of the top six most
695 enriched pathways, regulation of insulin-like growth factor and muscle contraction, have
696 proteins that play many roles during morphogenesis.
697
698 Insulin-like growth factor plays a role in a number of different developmental processes,
699 including odontogenesis, bone development, organ development, and brain
700 development (Baroncelli et al., 2017; Brown et al., 2017; Chen et al., 2009; Dodington et
701 al., 2021; Luo et al., 2020; Montivero et al., 2021; Oyanagi et al., 2019; Vassilakos et al.,
702 2019). Thus, regulation of IGF is a complex set of processes with many different factors
703 involved in regulating expression in different tissues. This includes regulation by thyroid
704 growth hormone (Yakar & Isaksson, 2016) and regulation via phosphorylation of binding
705 proteins to aid in transport, activation, and inhibition (Chrudinova et al., 2024; Dong et
706 al., 2022; Huttlin et al., 2010; Palma-Lara et al., 2023; Tagliabracci et al., 2015). Given

707 the importance of IGF to multiple developmental processes, regulation of IGF is a
708 probable candidate for a mechanism underlying phenotypic plasticity. Experimental
709 manipulation of IGF1 and IGF2 during odontogenesis has revealed systematic changes
710 to the size and number of cusps of developing molars (Oyanagi et al., 2019). The
711 connection between IGF1 and IGF2 gene expression and proteins associated with IGF
712 regulation, which includes Amelogenin X, is not currently well understood (Bansal et al.,
713 2012; Oyanagi et al., 2019; Pandya & Diekwisch, 2021). However, regulation of insulin-
714 like growth factor offers a promising pathway for future investigation, particularly in
715 elucidating responses of IGF gene expression and associated regulatory factors to
716 environmental perturbations, such as poor diet.
717
718 Similarly, our collection of proteins from the muscle contraction pathway are primarily
719 actin-based myosins. The function of myosins as motor proteins is well documented, but
720 the specific nature of how myosins interact during odontogenesis is poorly understood
721 (Du et al., 2024; Guhathakurta et al., 2018). Previous proteomic studies of teeth have
722 not reported differential expression of actin-based myosins, making this result
723 unexpected. Simultaneously, those studies were not attempting to experimentally
724 induce plastic responses like our study. The connection of actin-based myosins with
725 body size and potentially with amelogenesis imperfecta suggests that future
726 investigations may be fruitful. These future studies would hopefully confirm the results
727 we recovered and further explore the relationship between protein expression and
728 phenotypic plasticity.

Conclusions

Proteomic expression results supported our prediction that halving dietary protein during embryogenesis and early postnatal development would alter expression of proteins recovered from mouse molars. Specifically, we identified 120 differentially expressed proteins associated with a reduction of dietary protein during embryonic and early postnatal development. Changes in dietary protein have been proposed to result in phenotypically plastic changes in molar size and skull length. Our study did not recover significant differences between normal and low protein groups for either a measure of molar size or skull length. The discordance between positive proteomic results and negative phenotypic results suggests that phenotypic differences may be more nuanced that initially predicted.

We recovered significant changes in proteins associated with dental development, that are primarily within the pathway associated with regulation of Insulin-Like Growth Factor. The connection between IGF and dental proteins remains to be further investigated, but changes in expression in this pathway could directly influence tooth structure. We also identified systematically reduced expression for proteins in the Muscle contraction pathway, specifically actin-based myosins, a novel discovery for tooth-derived proteomics data. Actin-based myosins are broadly implicated in vertebrate development and are correlated with dental and general body development. Taken together, it is possible that we perturbed tooth phenotypes, such as enamel or dentin thickness or density, that are not captured by our measures of craniodental size.

752

753 Fortunately, the study presented here is part of a larger research program aimed at
754 more comprehensive phenotyping efforts. The results of this study will allow us to focus
755 on investigating phenotypic hypotheses derived from our proteomics results (e.g.,
756 testing for amelogenesis imperfecta). As well as continuing to investigate other aspects
757 of craniodental morphology, to include assessment of size of the second and third
758 molars and shape of all three molars, along with cranial traits such as depth and width
759 of the cranium. Inclusion of these more comprehensive phenotypic data may recover
760 differences between groups that were not recovered from the data reported here.
761

762 Our controlled feeding experiment also induced increased immune system activation
763 and inflammation response, as evidenced by increased expression of proteins in the
764 Neutrophil degranulation pathway. While this result does not directly inform us about
765 phenotypic plasticity, that we could potentially to derive such information from a fully
766 mineralized teeth could prove useful for studying the biology of deceased or extinct
767 organisms. New studies aimed at microsampling enamel, dentin, and along the enamel-
768 dentin junction to determine both the source of these signals and which tissues contain
769 them are necessary.
770

771 Finally, we propose that proteomic quantification of non-experimental organisms will
772 prove fruitful and predict that dietary changes in wild settings will change enamel and
773 dentin formation by altering aspects of the IGF regulatory pathway and potentially
774 expression of actin-based myosins. Future research efforts then should focus on

elucidating the connection between IGF gene expression and enamel and dentin protein expression; determining the role of actin-based myosins in tooth and skeletal development; and comparing the immune and inflammation signals in proteomic data to classically used tools (e.g., blood panels and cortisol screening). With a combination of phenotyping and proteomic investigations it will become clearer precisely what traits are more likely to be perturbed, and what sections of these pathways are causal to those changes. In turn, this will enhance the utility of quantitative proteomics for investigating organismal biology more broadly.

Acknowledgments

We thank the Stony Brook Division of Laboratory Animal Research (DLAR), particularly Laurie Levine, for animal husbandry and management. We thank Dr. John Haley of the Stony Brook University Proteomics Core Facility, for sample preparation and initial post-processing of proteomics data. We thank the New York Institute of Technology Visualization Center staff, Dr. Brian Beatty and Kelsi Hurdle, for providing technical support in scanning and reconstruction of µCT scans. We thank the Stony Brook University Center for Inclusive Education staff: Lisa Ospitale, Diana Champney, and Erica Valdez, and Stony Brook IRACDA PIs, Dr. Carol Carter and Karian Wright, for financial and administrative support.

Author RWB was funded via an Institutional Research and Academic Career Development Award (IRACDA) made to Stony Brook University from the National Institute of General Medical Sciences of the National Institutes of Health [K12GM102778], and startup funding to NSV from Stony Brook University. The content

is solely the responsibility of the authors and does not necessarily represent official views of the National Institutes of Health.

Cited

Adams, D. C., Otárola-Castillo, E., & Paradis, E. (2013). geomorph: anrpackage for the collection and analysis of geometric morphometric shape data. *Methods in Ecology and Evolution, 4*(4), 393-399. doi:10.1111/2041-210x.12035

Aioub, M., Lezot, F., Molla, M., Castaneda, B., Robert, B., Goubin, G., . . . Berdal, A. (2007). Msx2 -/- transgenic mice develop compound amelogenesis imperfecta, dentinogenesis imperfecta and periodental osteopetrosis. *Bone, 41*(5), 851-859. doi:10.1016/j.bone.2007.07.023

Al-Amrani, S., Al-Jabri, Z., Al-Zaabi, A., Alshekaili, J., & Al-Khabori, M. (2021). Proteomics: Concepts and applications in human medicine. *World J Biol Chem, 12*(5), 57-69. doi:10.4331/wjbc.v12.i5.57

Alghadeer, A., Hanson-Drury, S., Patni, A. P., Ehnes, D. D., Zhao, Y. T., Li, Z., . . . Ruohola-Baker, H. (2023). Single-cell census of human tooth development enables generation of human enamel. *Dev Cell, 58*(20), 2163-2180 e2169. doi:10.1016/j.devcel.2023.07.013

Bansal, A. K., Shetty, D. C., Bindal, R., & Pathak, A. (2012). Amelogenin: A novel protein with diverse applications in genetic and molecular profiling. *J Oral Maxillofac Pathol, 16*(3), 395-399. doi:10.4103/0973-029X.102495

Barbeito-Andrés, J., Gonzalez, P., & Hallgrímsson, B. (2016). Prenatal development of skull and brain in a mouse model of growth restriction. *Revista Argentina de Antropología Biológica, 18*(1). doi:10.17139/raab.2016.0018.01.05

Baroncelli, L., Cenni, M. C., Melani, R., Deidda, G., Landi, S., Narducci, R., . . . Berardi, N. (2017). Early IGF-1 primes visual cortex maturation and accelerates developmental switch between NKCC1 and KCC2 chloride transporters in enriched animals. *Neuropharmacology, 113*(Pt A), 167-177. doi:10.1016/j.neuropharm.2016.02.034

Bell, C. J., & Jass, C. N. (2011). Polyphyly, paraphyly, provinciality, and the promise of intercontinental correlation - Charles Repenning's contributions to the study of arvicoline rodent evolution and biochronology. *Palaeontologia Electronica, 14*(3), 15.

Brown, S. M., Peters, R., & Lawrence, A. B. (2017). Up-regulation of IGF-1 in the frontal cortex of piglets exposed to an environmentally enriched arena. *Physiol Behav, 173*, 285-292. doi:10.1016/j.physbeh.2017.02.030

Burroughs, R. W. (2019). Phylogenetic and Developmental Constraints Dictate the Number of Cusps on Molars in Rodents. *Sci Rep, 9*(1), 10902. doi:10.1038/s41598-019-47469-x

Chantada-Vazquez, M. D. P., Bravo, S. B., Barbosa-Gouveia, S., Alvarez, J. V., & Couce, M. L. (2022). Proteomics in Inherited Metabolic Disorders. *Int J Mol Sci, 23*(23). doi:10.3390/ijms232314744

Chen, J. H., Martin-Gronert, M. S., Tarry-Adkins, J., & Ozanne, S. E. (2009). Maternal protein restriction affects postnatal growth and the expression of key proteins involved in lifespan regulation in mice. *PLoS One, 4*(3), e4950. doi:10.1371/journal.pone.0004950

Choby, J. E., Monteith, A. J., Himmel, L. E., Margaritis, P., Shirey-Rice, J. K., Pruijssers, A., . . . Skaar, E. P. (2019). A Phenome-Wide Association Study Uncovers a Pathological Role of Coagulation Factor X during Acinetobacter baumannii Infection. *Infect Immun, 87*(5). doi:10.1128/IAI.00031-19

Chrudinova, M., Kirk, N. S., Chuard, A., Venugopal, H., Zhang, F., Lubos, M., . . . Altindis, E. (2024). A viral insulin-like peptide inhibits IGF-1 receptor phosphorylation and regulates IGF1R gene expression. *Mol Metab, 80*, 101863. doi:10.1016/j.molmet.2023.101863

Croft, D., O'Kelly, G., Wu, G., Haw, R., Gillespie, M., Matthews, L., . . . Stein, L. (2011). Reactome: a database of reactions, pathways and biological processes. *Nucleic Acids Res, 39*(Database issue), D691-697. doi:10.1093/nar/gkq1018

Dickerson, J. W. T., & Hughes, P. C. R. (1972). Growth of the rat skeleton after severe nutritional intrauterine and post-natal retardation. *Resuscitation, 1*(2), 163-170. doi:10.1016/0300-9572(72)90019-6

Dodington, D. W., Yumol, J. L., Yang, J., Pollock-Tahiri, E., Sivasubramaniyam, T., Sacco, S. M., . . . Woo, M. (2021). JAK2-IGF1 axis in osteoclasts regulates postnatal growth in mice. *JCI Insight, 6*(5). doi:10.1172/jci.insight.137045

Dong, C., Lamichhane, B., Yamazaki, H., Vasquez, B., Wang, J., Zhang, Y., . . . Wang, X. (2022). The phosphorylation of serine(55) in enamelin is essential for murine amelogenesis. *Matrix Biol, 111*, 245-263. doi:10.1016/j.matbio.2022.07.001

Du, W., Verma, A., Ye, Q., Du, W., Lin, S., Yamanaka, A., . . . Hu, J. K. (2024). Myosin II mediates Shh signals to shape dental epithelia via control of cell adhesion and movement. *PLoS Genet, 20*(6), e1011326. doi:10.1371/journal.pgen.1011326

Duverger, O., & Morasso, M. I. (2018). Pleiotropic function of DLX3 in amelogenesis: from regulating pH and keratin expression to controlling enamel rod decussation. *Connect Tissue Res, 59*(sup1), 30-34. doi:10.1080/03008207.2017.1408602

Eichelberger, K. R., & Goldman, W. E. (2020). Manipulating neutrophil degranulation as a bacterial virulence strategy. *PLoS Pathog, 16*(12), e1009054. doi:10.1371/journal.ppat.1009054

Fedorov, A., Beichel, R., Kalpathy-Cramer, J., Finet, J., Fillion-Robin, J. C., Pujol, S., . . . Kikinis, R. (2012). 3D Slicer as an image computing platform for the Quantitative Imaging Network. *Magn Reson Imaging, 30*(9), 1323-1341. doi:10.1016/j.mri.2012.05.001

Freeman, T., Dixon, A., Campbell, E., Tait, T., Richardson, P., Rice, K., . . . Bentley, D. (1998). *Expression Mapping of Mouse Genes*.

Froment, C., Zanolli, C., Hourset, M., Mouton-Barbosa, E., Moreira, A., Burlet-Schiltz, O., & Mollereau, C. (2021). Protein sequence comparison of human and non-human primate tooth proteomes. *J Proteomics, 231*, 104045. doi:10.1016/j.jprot.2020.104045

Giovani, P. A., Martins, L., Salmon, C. R., Mofatto, L. S., Leme, A. F. P., Puppin-Rontani, R. M., . . . Kantovitz, K. R. (2021). Comparative proteomic analysis of dental cementum from deciduous and permanent teeth. *J Periodontal Res, 56*(1), 173-185. doi:10.1111/jre.12808

Green, D. R., Schulte, F., Lee, K. H., Pugach, M. K., Hardt, M., & Bidlack, F. B. (2019). Mapping the Tooth Enamel Proteome and Amelogenin Phosphorylation Onto Mineralizing Porcine Tooth Crowns. *Front Physiol, 10*, 925. doi:10.3389/fphys.2019.00925

Guhathakurta, P., Prochniewicz, E., & Thomas, D. D. (2018). Actin-Myosin Interaction: Structure, Function and Drug Discovery. *Int J Mol Sci, 19*(9). doi:10.3390/ijms19092628

Harjunmaa, E., Seidel, K., Hakkinen, T., Renvoise, E., Corfe, I. J., Kallonen, A., . . . Jernvall, J. (2014). Replaying evolutionary transitions from the dental fossil record. *Nature, 512*(7512), 44-48. doi:10.1038/nature13613

Heck, M., & Neely, B. A. (2020). Proteomics in Non-model Organisms: A New Analytical Frontier. *J Proteome Res, 19*(9), 3595-3606. doi:10.1021/acs.jproteome.0c00448

Holloway, P. J., Shaw, J. H., & Swenney, E. A. (1961). EFFECTS OF VARIOUS SUCROSE:CASEIN RATIOS IN PURIFIED DIETS ON THE TEETH AND SUPPORTING STRUCTURES OF RATS. *Arch Oral Biol, 3*, 185-200.

Hopkins, S. S. B. (2018). Estimation of Body Size in Fossil Mammals. In D. A. Croft, D. F. Su, & S. W. Simpson (Eds.), *Methods in Paleoecology: Reconstructing Cenozoic Terrestrial Environments and Ecological Communities* (pp. 7-22). Cham: Springer International Publishing.

Huttlin, E. L., Jedrychowski, M. P., Elias, J. E., Goswami, T., Rad, R., Beausoleil, S. A., . . . Gygi, S. P. (2010). A tissue-specific atlas of mouse protein phosphorylation and expression. *Cell, 143*(7), 1174-1189. doi:10.1016/j.cell.2010.12.001

Immel, A., Le Cabec, A., Bonazzi, M., Herbig, A., Temming, H., Schuenemann, V. J., . . . Krause, J. (2016). Effect of X-ray irradiation on ancient DNA in sub-fossil bones - Guidelines for safe X-ray imaging. *Sci Rep, 6*, 32969. doi:10.1038/srep32969

Jagr, M., Ergang, P., Pataridis, S., Kolrosova, M., Bartos, M., & Miksik, I. (2019). Proteomic analysis of dentin-enamel junction and adjacent protein-containing enamel matrix layer of healthy human molar teeth. *Eur J Oral Sci, 127*(2), 112-121. doi:10.1111/eos.12594

Levis, N. A., & Pfennig, D. W. (2021). Innovation and Diversification Via Plasticity-Led Evolution. In *Phenotypic Plasticity & Evolution* (pp. 211-240).

Liu, C., & Zhang, R. (2021). Biomineral proteomics: A tool for multiple disciplinary studies. *J Proteomics, 238*, 104171. doi:10.1016/j.jprot.2021.104171

Lobe, S. L., Bernstein, M. C., & German, R. Z. (2006). Life-long protein malnutrition in the rat (Rattus norvegicus) results in altered patterns of craniofacial growth and smaller individuals. *J Anat, 208*(6), 795-812. doi:10.1111/j.1469-7580.2006.00565.x

Luis, N. M., & Schnorrer, F. (2021). Mechanobiology of muscle and myofibril morphogenesis. *Cells Dev, 168*, 203760. doi:10.1016/j.cdev.2021.203760

Luo, Y., Liu, Z., Luo, S., Wang, X., & Tao, L. (2020). The developmental and experience-dependent expression of IGF-2 in mice visual cortex. *Neurosci Lett, 721*, 134828. doi:10.1016/j.neulet.2020.134828

McCance, R. A., Ford, E. H., & Brown, W. A. (1961). Severe undernutrition in growing and adult animals. 7. Development of the skull, jaws and teeth in pigs. *Br J Nutr, 15*, 213-224. doi:10.1079/bjn19610026

Mehta, S., Bernt, M., Chambers, M., Fahrner, M., Foll, M. C., Gruening, B., . . . Griffin, T. J. (2023). A Galaxy of informatics resources for MS-based proteomics. *Expert Rev Proteomics, 20*(11), 251-266. doi:10.1080/14789450.2023.2265062

Miller, J. P., & German, R. Z. (1999). Protein Malnutrition Affects the Growth Trajectories of the Craniofacial Skeleton in Rats. *Journal of Nutrition, 129*, 2061-2069.

Molloy, M. P., Hill, C., McKay, M. J., & Herbert, B. R. (2023). Proteome Analysis of Whole Blood Collected by Volumetric Absorptive Microsampling. In D. W. Greening & R. J. Simpson (Eds.), *Serum/Plasma Proteomics: Methods and Protocols* (pp. 173-179). New York, NY: Springer US.

Montivero, A. J., Ghersi, M. S., Silvero, C. M., Artur de la Villarmois, E., Catalan-Figueroa, J., Herrera, M., . . . Perez, M. F. (2021). Early IGF-1 Gene Therapy Prevented Oxidative Stress and Cognitive Deficits Induced by Traumatic Brain Injury. *Front Pharmacol, 12*, 672392. doi:10.3389/fphar.2021.672392

Mukhtar, U., Goyal, A., Luthra-Guptasarma, M., Gauba, K., Kapur, A., & Thakur, A. K. (2022). Label-free quantitative proteomics reveals molecular correlates of altered biomechanical properties in molar incisor hypomineralization (MIH): an in vitro study. *Eur Arch Paediatr Dent, 23*(1), 179-191. doi:10.1007/s40368-021-00687-2

Muntel, J., Boswell, S. A., Tang, S., Ahmed, S., Wapinski, I., Foley, G., . . . Springer, M. (2015). Abundance-based classifier for the prediction of mass spectrometric peptide detectability upon enrichment (PPA). *Mol Cell Proteomics, 14*(2), 430-440. doi:10.1074/mcp.M114.044321

Nanci, A. (2007). Development of the Tooth and Its Supporting Tissues. In *Ten Cate's Oral Histology: Development, Structure, and Function* (pp. 79-107). St. Louis: Elsevier.

Orsini, G., Majorana, A., Mazzoni, A., Putignano, A., Falconi, M., Polimeni, A., & Breschi, L. (2014). Immunocytochemical detection of dentin matrix proteins in primary teeth from patients with dentinogenesis imperfecta associated with osteogenesis imperfecta. *Eur J Histochem, 58*(4), 2405. doi:10.4081/ejh.2014.2405

Othman, A., Sekheri, M., & Filep, J. G. (2022). Roles of neutrophil granule proteins in orchestrating inflammation and immunity. *FEBS J, 289*(14), 3932-3953. doi:10.1111/febs.15803

Oyanagi, T., Takeshita, N., Hara, M., Ikeda, E., Chida, T., Seki, D., . . . Takano-Yamamoto, T. (2019). Insulin-like growth factor 1 modulates bioengineered tooth morphogenesis. *Sci Rep, 9*(1), 368. doi:10.1038/s41598-018-36863-6

Palma-Lara, I., Garcia Alonso-Themann, P., Perez-Duran, J., Godinez-Aguilar, R., Bonilla-Delgado, J., Gomez-Archila, D., . . . Palacios-Reyes, C. (2023). Potential Role of Protein Kinase FAM20C on the Brain in Raine Syndrome, an In Silico Analysis. *Int J Mol Sci, 24*(10). doi:10.3390/ijms24108904

Pandya, M., & Diekwisch, T. G. H. (2021). Amelogenesis: Transformation of a protein-mineral matrix into tooth enamel. *J Struct Biol, 213*(4), 107809. doi:10.1016/j.jsb.2021.107809

Pandya, M., Liu, H., Dangaria, S. J., Zhu, W., Li, L. L., Pan, S., . . . Diekwisch, T. G. H. (2017). Integrative Temporo-Spatial, Mineralogic, Spectroscopic, and Proteomic Analysis of Postnatal Enamel Development in Teeth with Limited Growth. *Front Physiol, 8*, 793. doi:10.3389/fphys.2017.00793

Patton, J. L., & Brylski, P. V. (1987). Pocket Gophers in Alfalfa Fields: Causes and Consequences of Habitat-Related Body Size Variation. *The American Naturalist, 130*(4), 493-506.

Paynter, K. J., & Grainer, R. M. (1956). The relation of nutrition to the morphology and size of rat molar teeth. *journal of the Canadian Dental Association, 22*(9), 519-531.

Paynter, K. J., & Grainer, R. M. (1961). Influence of Nutrition and Genetics on Morphology and Caries Susceptibility. *Journal of the American Medical Association, 177*(5), 306-309.

Porto, A., Rolfe, S., & Maga, A. M. (2021). ALPACA: A fast and accurate computer vision approach for automated landmarking of three-dimensional biological structures. *Methods Ecol Evol, 12*(11), 2129-2144. doi:10.1111/2041-210X.13689

Procopio, N., Chamberlain, A. T., & Buckley, M. (2018). Exploring Biological and Geological Age-related Changes through Variations in Intra- and Intertooth Proteomes of Ancient Dentine. *J Proteome Res, 17*(3), 1000-1013. doi:10.1021/acs.jproteome.7b00648

Pucciarelli, H. M. (1980). The effects of race, sex, and nutrition on craniofacial differeniation in rats. A multivariate analysis. *Am J Phys Anthropol, 53*(3), 359-368. doi:10.1002/ajpa.1330530307

Pucciarelli, H. M. (1981). Growth of the functional components of the rat skull and its alteration by nutritional effects. A multivariate analysis. *Am J Phys Anthropol, 56*(1), 33-41. doi:10.1002/ajpa.1330560104

RCoreTeam. (2023). R: A Language and Environment for Statistical Computing. In. Vienna, Austria: R Foundation for Statistical Computing.

Rebeaud, M. E., Mallik, S., Goloubinoff, P., & Tawfik, D. S. (2021). On the evolution of chaperones and cochaperones and the expansion of proteomes across the Tree of Life. *Proc Natl Acad Sci U S A, 118*(21). doi:10.1073/pnas.2020885118

Ritchie, H. (2018). The functional significance of dentin sialoprotein-phosphophoryn and dentin sialoprotein. *Int J Oral Sci, 10*(4), 31. doi:10.1038/s41368-018-0035-9

Rolfe, S., Pieper, S., Porto, A., Diamond, K., Winchester, J., Shan, S., . . . Maga, A. M. (2021). SlicerMorph: An open and extensible platform to retrieve, visualize and analyze 3D morphology. *Methods Ecol Evol, 12*(10), 1816-1825. doi:10.1111/2041-210x.13669

Sartoretto, S., Gemini-Piperni, S., da Silva, R. A., Calasans, M. D., Rucci, N., Pires Dos Santos, T. M., . . . Zambuzzi, W. F. (2019). Apoptosis-associated speck-like protein containing a caspase-1 recruitment domain (ASC) contributes to osteoblast differentiation and osteogenesis. *J Cell Physiol, 234*(4), 4140-4153. doi:10.1002/jcp.27226

Searle, A. G. (1954). The Influence of Diet on Variation within Pure Lines. In *Genetical Studies on the Skeleton of the Mouse* (pp. 413-424).

Sharma, V., Rastogi, S., Kumar Bhati, K., Srinivasan, A., Roychoudhury, A., Nikolajeff, F., & Kumar, S. (2020). Mapping the Inorganic and Proteomic Differences among Different Types of Human Teeth: A Preliminary Compositional Insight. *Biomolecules, 10*(11). doi:10.3390/biom10111540

Shaw, J. H., & Griffiths, D. (1963). Dental Abnormalities in Rats Attributable to Protein Deficiency During Reproduction. *Journal of Nutrition, 80*, 123-141.

Shi, C., Ma, N., Zhang, W., Ye, J., Shi, H., Xiang, D., . . . Liu, Q. (2020). Haploinsufficiency of Dspp Gene Causes Dentin Dysplasia Type II in Mice. *Frontiers in Physiology, 11*. doi:10.3389/fphys.2020.593626

Steward, K. F., Refai, M., Dyer, W. E., Copie, V., Lachowiec, J., & Bothner, B. (2023). Acute stress reduces population-level metabolic and proteomic variation. *BMC Bioinformatics, 24*(1), 87. doi:10.1186/s12859-023-05185-4

Tagliabracci, V. S., Wiley, S. E., Guo, X., Kinch, L. N., Durrant, E., Wen, J., . . . Dixon, J. E. (2015). A Single Kinase Generates the Majority of the Secreted Phosphoproteome. *Cell, 161*(7), 1619-1632. doi:10.1016/j.cell.2015.05.028

Ungar, P. S. (2010). *Mammal Teeth: Origin, Evolution, and Diversity*. Baltimore: Johns Hopkins University Press.

Vassilakos, G., Lei, H., Yang, Y., Puglise, J., Matheny, M., Durzynska, J., . . . Barton, E. R. (2019). Deletion of muscle IGF-I transiently impairs growth and progressively disrupts glucose homeostasis in male mice. *FASEB J, 33*(1), 181-194. doi:10.1096/fj.201800459R

Visel, A., Thaller, C., & Eichele, G. (2004). GenePaint.org: an atlas of gene expression patterns in the mouse embryo. *Nucleic Acids Res, 32*(Database issue), D552-556. doi:10.1093/nar/gkh029

Wan, C., Yuan, G., Luo, D., Zhang, L., Lin, H., Liu, H., . . . Chen, Z. (2016). The Dentin Sialoprotein (DSP) Domain Regulates Dental Mesenchymal Cell Differentiation through a Novel Surface Receptor. *Sci Rep, 6*, 29666. doi:10.1038/srep29666

Wang, S., Song, R., Wang, Z., Jing, Z., Wang, S., & Ma, J. (2018). S100A8/A9 in Inflammation. *Front Immunol, 9*, 1298. doi:10.3389/fimmu.2018.01298

Wang, Z., Liu, P. K., & Li, L. (2024). A Tutorial Review of Labeling Methods in Mass Spectrometry-Based Quantitative Proteomics. *ACS Meas Sci Au, 4*(4), 315-337. doi:10.1021/acsmeasuresciau.4c00007

Weber, E. M., & Olsson, I. A. S. (2008). Maternal behaviour in Mus musculus sp.: An ethological review. *Applied Animal Behaviour Science, 114*(1-2), 1-22. doi:10.1016/j.applanim.2008.06.006

Wickham, H. (2016). *ggplot2: Elegant Graphics for Data Analysis*. New York: Springer-Verlag.

Wittmann, N., Behrendt, A. K., Mishra, N., Bossaller, L., & Meyer-Bahlburg, A. (2021). Instructions for Flow Cytometric Detection of ASC Specks as a Readout of Inflammasome Activation in Human Blood. *Cells, 10*(11). doi:10.3390/cells10112880

Wu, T., Hu, E., Xu, S., Chen, M., Guo, P., Dai, Z., . . . Yu, G. (2021). clusterProfiler 4.0: A universal enrichment tool for interpreting omics data. *Innovation (Camb), 2*(3), 100141. doi:10.1016/j.xinn.2021.100141

Yakar, S., & Isaksson, O. (2016). Regulation of skeletal growth and mineral acquisition by the GH/IGF-1 axis: Lessons from mouse models. *Growth Horm IGF Res, 28*, 26-42. doi:10.1016/j.ghir.2015.09.004

Yin, C., & Heit, B. (2018). Armed for destruction: formation, function and trafficking of neutrophil granules. *Cell Tissue Res, 371*(3), 455-471. doi:10.1007/s00441-017-2731-8

Zougman, A., Wilson, J. P., & Banks, R. E. (2020). A simple serum depletion method for proteomics analysis. *Biotechniques, 69*(2), 148-151. doi:10.2144/btn-2020-0017

Graphical Abstract:

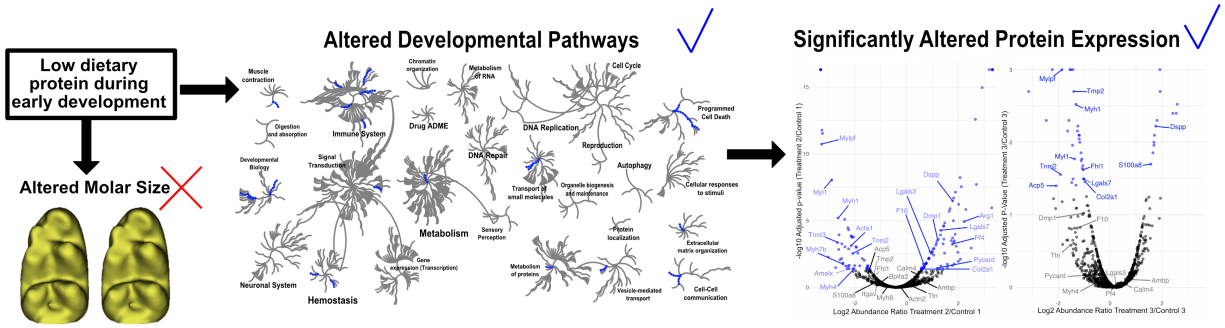

Following Page

Figure 1: Models of skulls of treatment specimens used for proteomic sampling and processed from µCT scans. A: Lateral and Ventral view of skull, showing where right upper M1 was removed, M2 and M3 are still visible. Light blue shows M1 still in place, Fuschia dots indicate where roots for M1 once inserted. B: Dorsal view of skull, opacity adjusted to 50% to show location of landmarks for straight-line skull estimate. C: Scheme of 25 landmarks placed on left lower m1 used to assess crown area and shape between treatment and control specimens.

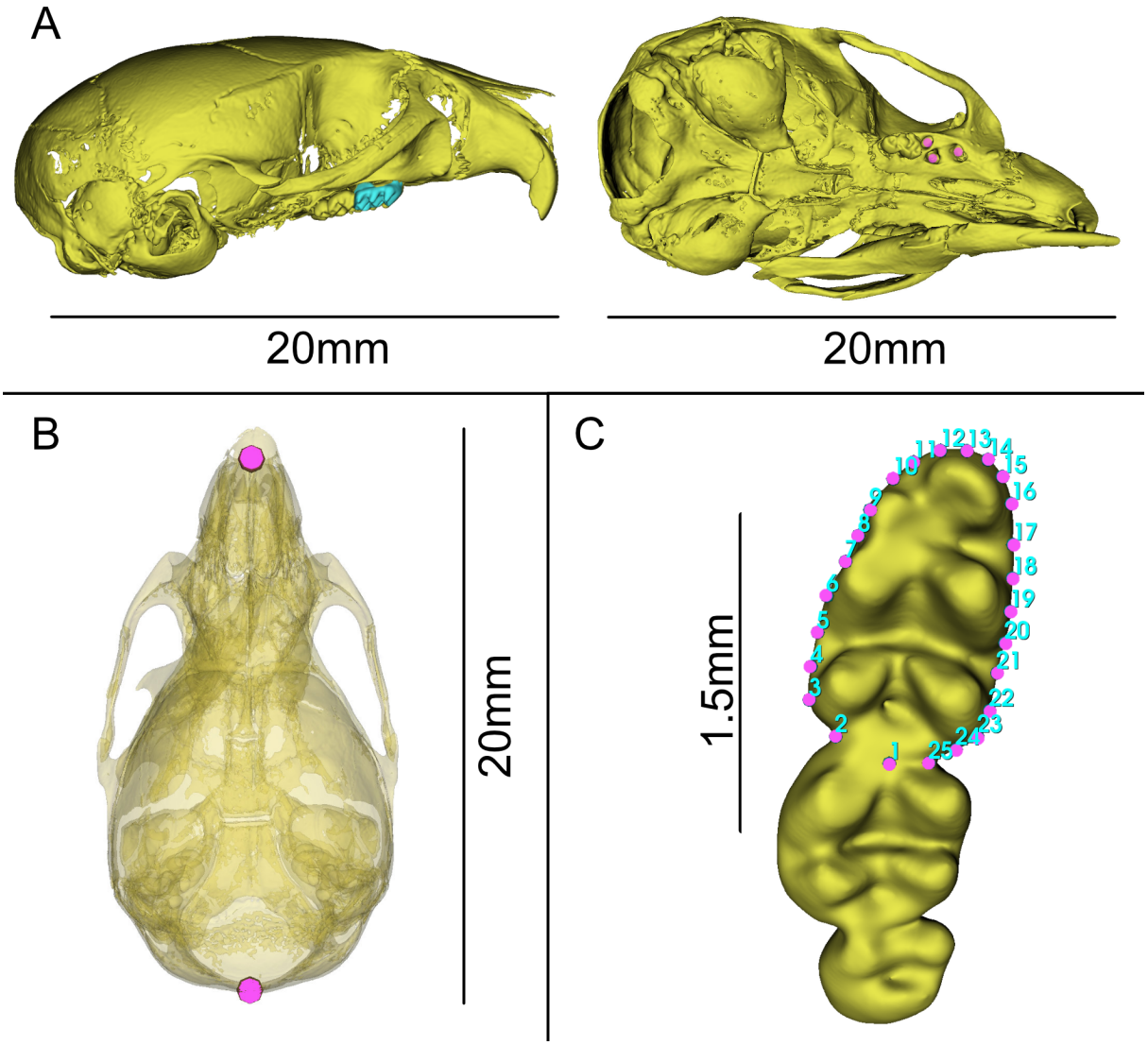
A
20mm
20mm
B
20mm
C
1.5mm
1
2
3
4
5
6
7
8
9
10
11
12
13
14
15
16
17
18
19
20
21
22
23
24
25

Figure 2: Results of phenotypic investigation. A: Estimates of straight line skull length. B: Estimates of crown area.

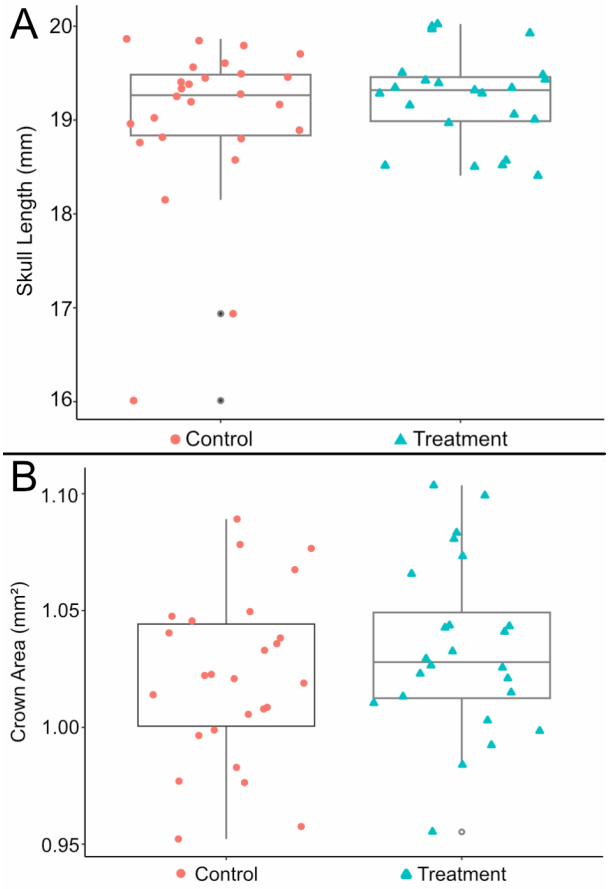

Following Page

Figure 3: Most enriched pathways from Gene Ontology (GO) analysis of CGSig. A: Biological Processes, B: Cellular Components, C: Metabolic Function

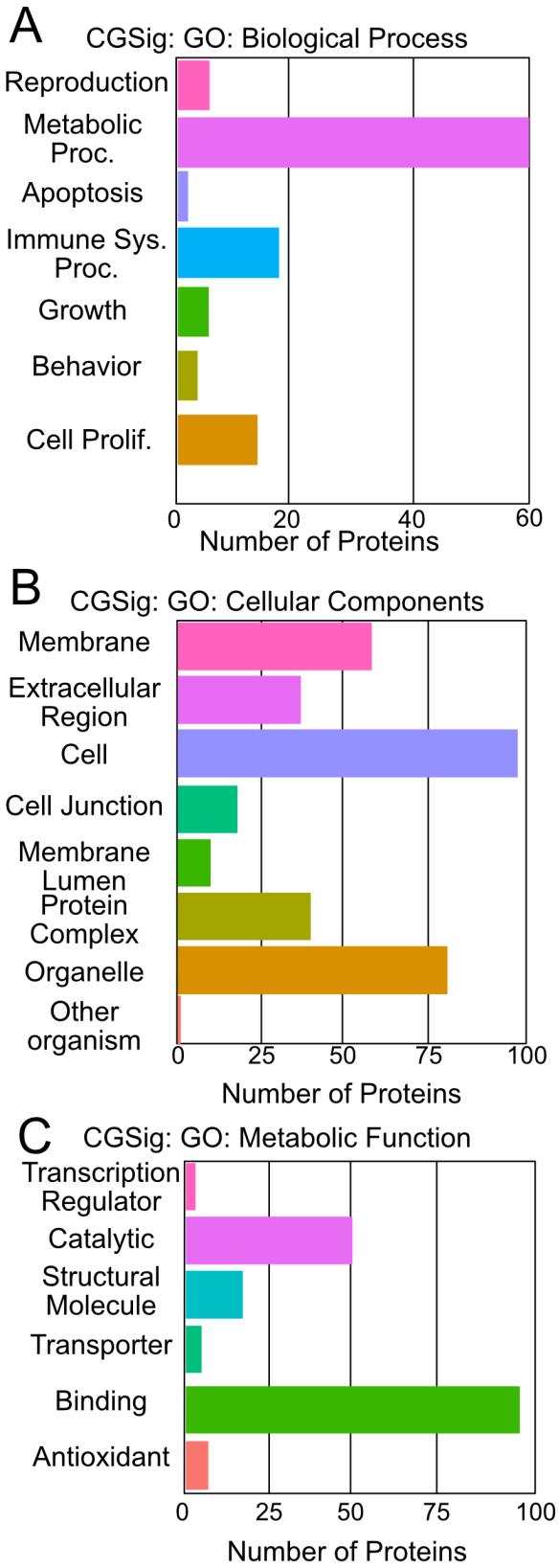
A
CGSig: GO: Biological Process
Reproduction
Metabolic Proc.
Apoptosis
Immune Sys. Proc.
Growth
Behavior
Cell Prolif.
0
20
40
60
Number of Proteins
B
CGSig: GO: Cellular Components
Membrane
Extracellular Region
Cell
Cell Junction
Membrane Lumen
Protein Complex
Organelle
Other organism
0
25
50
75
100
Number of Proteins
C
CGSig: GO: Metabolic Function
Transcription Regulator
Catalytic
Structural Molecule
Transporter
Binding
Antioxidant
0
25
50
75
100
Number of Proteins

Figure 4: Volcano of specimen proteomics data exemplified by selected comparison from each group. A: From Group 1 Treatment 2 over Control 1. B: From Group 2 Treatment 3 over Control 4. Blue dots show Adjusted Abundance Ratio P-values ≤ 0.05. Labeled dots are proteins related to osteogenesis, odontogenesis, inflammation and immune response, and muscle contraction. Volcano plots of remaining 6 comparisons are provided in Supplemental Materials.

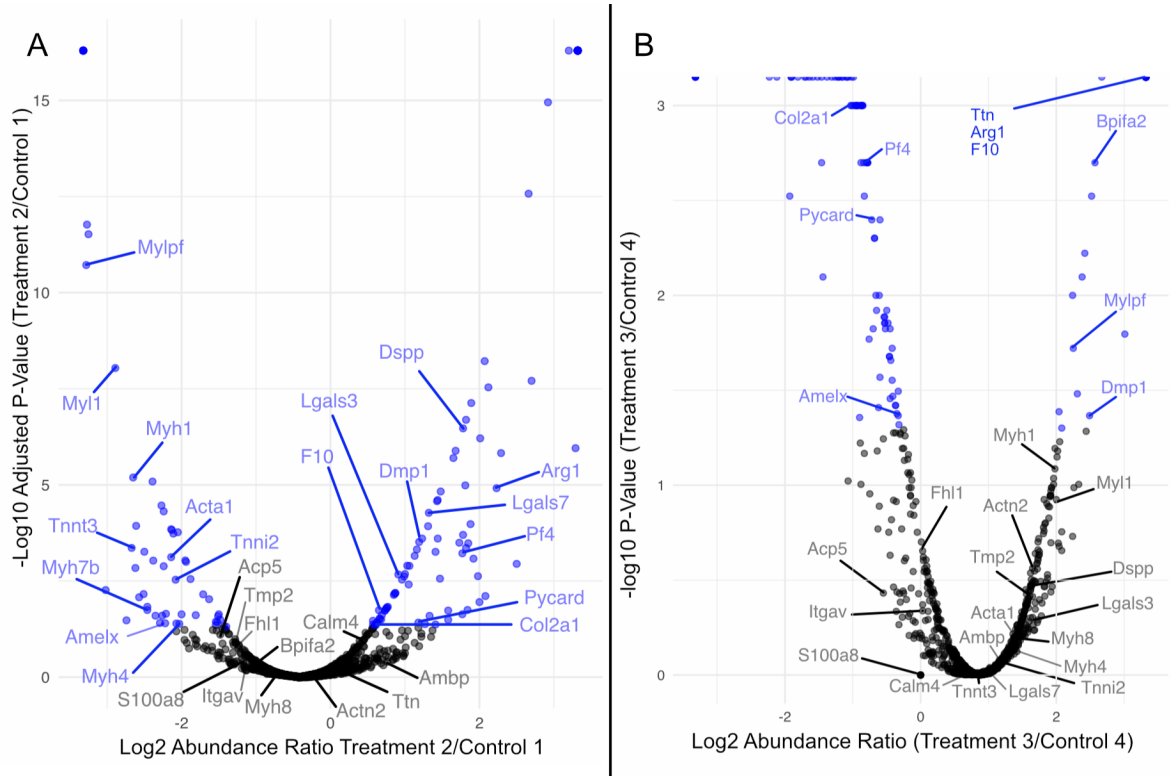

Table 1: List of proteins with significant differential expression between low dietary protein (10%) treatment and normal dietary protein (20%) control groups. Average Log2 fold change calculated by averaging of specimens with significant change of abundance ratio (SI 1). Up=Significant specimens have positive Log2 fold change meaning increased expression of that protein. Down = Specimens have negative Log2 fold change meaning decreased expression of that protein. Proteins with blank averages are where a consistent signal was not identified due to individual variation. The number of specimens which could be individually interpreted as Up (U) or Down (D) is provided. Data are from SI 1.

Uniprot Accession	Protein and Gene Name	GO: Process	Avg. Log2	Up/ Down
P63277	Amelogenin, X isoform GN=Amelx	Odontogenesis	-1.52	Down
O55188	Dentin matrix acidic phosphoprotein 1 GN=Dmp1	Odontogenesis		3U/2D
P97399	Dentin sialophosphoprotein GN=Dspp	Odontogenesis	1.77	Up
P43406	Integrin alpha-V GN=Itgav	Osteogenesis	-2.66	Down
Q05117	Tartrate-resistant acid phosphatase type 5 GN=Acp5	Osteogenesis	-1.71	Down
P28481	Collagen alpha-1(II) chain GN=Col2a1	Osteogenesis		1U/2D
O54974	Galectin-7 GN=Lgals7	Osteogenesis		3U/2D
P27005	Protein S100-A8 GN=S100a8	Inflammation and Immune Response	-1.27	Down
O88947	Coagulation factor X GN=F10	Inflammation and Immune Response	-0.23	Down
Q9EPB4	Apoptosis-associated speck-like protein containing a CARD GN=Pycard	Inflammation and Immune Response		1U/1D
Q9JM83	Calmodulin-4 GN=Calm4	Inflammation and Immune Response		2U/1D
Q9Z126	Platelet factor 4 GN=Pf4	Inflammation and Immune Response	0.92	Up
P16110	Galectin-3 GN=Lgals3	Inflammation and Immune Response	1.10	Up
P07743	BPI fold-containing family A member 2 GN=Bpifa2	Inflammation and Immune Response	1.50	Up
Q07456	Protein AMBP GN=Ambp	Inflammation and Immune Response	2.30	Up
Q61176	Arginase-1 GN=Arg1	Inflammation and Immune Response	2.40	Up
Q9JJZ2	Tubulin alpha-8 chain GN=Tuba8	Cytoskeleton Formation	-2.29	Down
Q8R1Q8	Cytoplasmic dynein 1 light intermediate chain 1 GN=Dync1li1	Cytoskeleton Formation	-1.59	Down
Q9CRB9	MICOS complex subunit Mic19 GN=Chchd3	Cytoskeleton Formation	-1.17	Down
Q91ZU6	Dystonin GN=Dst	Cytoskeleton Formation	-0.56	Down
P08032	Spectrin alpha chain, erythrocytic 1 GN=Spta1	Cytoskeleton Formation		1U/1D
Q61554	Fibrillin-1 GN=Fbn1	Cytoskeleton Formation	0.09	Up
P15508	Spectrin beta chain, erythrocytic GN=Sptb	Cytoskeleton Formation		1U/1D
P55292	Desmocollin-2 GN=Dsc2	Cytoskeleton Formation		2U/1D
P48193	Protein 4.1 GN=Epb41	Cytoskeleton Formation		2U/1D
P10637	Microtubule-associated protein tau GN=Mapt	Cytoskeleton Formation	1.07	Up
O35902	Desmoglein-3 GN=Dsg3	Cytoskeleton Formation	1.20	Up
Q7TSF1	Desmoglein-1-beta GN=Dsg1b	Cytoskeleton Formation	1.22	Up
P97350	Plakophilin-1 GN=Pkp1	Cytoskeleton Formation	1.58	Up
Q02257	Junction plakoglobin GN=Jup	Cytoskeleton Formation	1.65	Up
E9Q557	Desmoplakin GN=Dsp	Cytoskeleton Formation	1.80	Up
G5E8K5	Ankyrin-3 GN=Ank3	Cytoskeleton Formation	1.87	Up
Q3UV17	Keratin, type II cytoskeletal 2 oral GN=Krt76	Development of Cornified Envelope		3U/2D
A1L317	Keratin, type I cytoskeletal 24 GN=Krt24	Development of Cornified Envelope	0.76	Up
P04104	Keratin, type II cytoskeletal 1 GN=Krt1	Development of Cornified Envelope	1.26	Up
Q61781	Keratin, type I cytoskeletal 14 GN=Krt14	Development of Cornified Envelope	1.46	Up
P97347	Repetin GN=Rptn	Development of Cornified Envelope	1.47	Up
Q61414	Keratin, type I cytoskeletal 15 GN=Krt15	Development of Cornified Envelope	1.51	Up
Q09PK2	Retroviral-like aspartic protease 1 GN=Asprv1	Development of Cornified Envelope	1.70	Up
Q62266	Cornifin-A GN=Sprr1a	Development of Cornified Envelope	1.75	Up
A6BLY7	Keratin, type I cytoskeletal 28 GN=Krt28	Development of Cornified Envelope	1.89	Up
Q62267	Cornifin-B GN=Sprr1b	Development of Cornified Envelope	2.93	Up
A2AQP0	Myosin-7B GN=Myh7b	Muscle Contraction	-2.37	Down
Q9QZ47	Troponin T, fast skeletal muscle GN=Tnnt3	Muscle Contraction	-2.34	Down

Q5SX39	Myosin-4 GN=Myh4	Muscle Contraction	-2.25	Down
P13542	Myosin-8 GN=Myh8	Muscle Contraction	-2.24	Down
Q5SX40	Myosin-1 GN=Myh1	Muscle Contraction	-1.91	Down
P05977	Myosin light chain 1/3, skeletal muscle isoform GN=Myl1	Muscle Contraction	-1.88	Down
P68134	Actin, alpha skeletal muscle GN=Acta1	Muscle Contraction	-1.86	Down
Q3SX28	TREMBL:Q3SX28;Q5KR48 (Bos taurus) Tropomyosin 2	Muscle Contraction	-1.61	Down
P13412	Troponin I, fast skeletal muscle GN=Tnni2	Muscle Contraction	-1.59	Down
P97457	Myosin regulatory light chain 2, skeletal muscle isoform GN=Mylpf	Muscle Contraction	-1.42	Down
P97447	Four and a half LIM domains protein 1 GN=Fhl1	Muscle Contraction	-1.06	Down
A2ASS6	Titin GN=Ttn	Muscle Contraction	-0.80	Down
Q9JI91	Alpha-actinin-2 GN=Actn2	Muscle Contraction	-0.48	Down
P07310	Creatine kinase M-type GN=Ckm	Phosphorylation	-2.03	Down
P28650	Adenylosuccinate synthetase isozyme 1 GN=Adssl1	Phosphorylation	-1.24	Down
Q9R0Y5	Adenylate kinase isoenzyme 1 GN=Ak1	Phosphorylation	-0.71	Down
P29699	Alpha-2-HS-glycoprotein GN=Ahsg	Phosphorylation		2U/1D
Q9R0H0	Peroxisomal acyl-coenzyme A oxidase 1 GN=Acox1	Regulation	-2.12	Down
P63330	Serine/threonine-protein phosphatase 2A GN=Ppp2ca	Regulation	-1.78	Down
Q9EST5	Acidic leucine-rich nuclear phosphoprotein 32 B GN=Anp32b	Regulation	-1.18	Down
P07759	Serine protease inhibitor A3K GN=Serpina3k	Regulation	-1.17	Down
P28665	Murinoglobulin-1 GN=Mug1	Regulation	-0.88	Down
Q9Z2N8	Actin-like protein 6A GN=Actl6a	Regulation	-0.62	Down
O55042	Alpha-synuclein GN=Snca	Regulation	0.29	Up
Q5FWK3	Rho GTPase-activating protein 1 GN=Arhgap1	Regulation		1U/1D
Q9D5V5	Cullin-5 GN=Cul5	Regulation	0.38	Down
Q6P253	Dermokine GN=Dmkn	Regulation	0.89	Up
Q08189	Protein-glutamine gamma-glutamyltransferase E GN=Tgm3	Regulation	1.04	Up
Q60604	Adseverin GN=Scin	Regulation	1.32	Up
Q9D2Q8	Protein S100-A14 GN=S100a14	Regulation	1.45	Up
Q8CGR5	Kallikrein-14 GN=Klk14	Regulation	1.55	Up
P21570	Angiogenin GN=Ang	Regulation	2.42	Up
Q62203	Splicing factor 3A subunit 2 GN=Sf3a2	Transcription and Repair	-0.21	Down
Q9R0Q6	Actin-related protein 2/3 complex subunit 1A GN=Arpc1a	Transcription and Repair	2.09	Up
P32848	Parvalbumin alpha GN=Pvalb	Binding	-2.24	Down
P62631	Elongation factor 1-alpha 2 GN=Eef1a2	Binding	-2.01	Down
O35744	Chitinase-like protein 3 GN=Chil3	Binding	-1.82	Down
P31786	Acyl-CoA-binding protein GN=Dbi	Binding	-1.72	Down
P81117	Nucleobindin-2 GN=Nucb2	Binding	-1.09	Down
O70456	14-3-3 protein sigma GN=Sfn	Binding	1.09	Up
P63024	Vesicle-associated membrane protein 3 GN=Vamp3	Transport	-3.07	Down
Q9JLM8	Serine/threonine-protein kinase DCLK1 GN=Dclk1	Transport	-2.40	Down
P18872	Guanine nucleotide-binding protein G(o) subunit alpha GN=Gnao1	Transport	-2.35	Down
Q8VEH3	ADP-ribosylation factor-like protein 8A GN=Arl8a	Transport	-2.18	Down
P61028	Ras-related protein Rab-8B GN=Rab8b	Transport	-2.07	Down
P04247	Myoglobin GN=Mb	Transport	-1.71	Down
P02089	Hemoglobin subunit beta-2 GN=Hbb-b2	Transport	-1.51	Down

P04117	Fatty acid-binding protein, adipocyte GN=Fabp4	Transport	-1.16	Down
P02088	Hemoglobin subunit beta-1 GN=Hbb-b1	Transport		1U/1D
P04919	Band 3 anion transport protein GN=Slc4a1	Transport		1U/1D
P97449	Aminopeptidase N GN=Anpep	Transport		1U/1D
P14602	Heat shock protein beta-1 GN=Hspb1	Transport	1.44	Up
P24668	Cation-dependent mannose-6-phosphate receptor GN=M6pr	Transport	2.37	Up
Q8VHI3	GDP-fucose protein O-fucosyltransferase 2 GN=Pofut2	Metabolism	-2.35	Down
Q5SWU9	Acetyl-CoA carboxylase 1 GN=Acaca	Metabolism	-2.03	Down
Q9D2R0	Acetoacetyl-CoA synthetase GN=Aacs	Metabolism	-1.93	Down
O70503	Very-long-chain 3-oxoacyl-CoA reductase GN=Hsd17b12	Metabolism	-1.87	Down
P19096	Fatty acid synthase GN=Fasn	Metabolism	-1.83	Down
P21550	Beta-enolase GN=Eno3	Metabolism	-1.77	Down
O70250	Phosphoglycerate mutase 2 GN=Pgam2	Metabolism	-1.75	Down
Q8R429	Sarcoplasmic/endoplasmic reticulum calcium ATPase 1 GN=Atp2a1	Metabolism	-1.73	Down
Q9EQ06	Estradiol 17-beta-dehydrogenase 11 GN=Hsd17b11	Metabolism	-1.38	Down
P13634	Carbonic anhydrase 1 GN=Ca1	Metabolism	-0.92	Down
Q9WUB3	Glycogen phosphorylase, muscle form GN=Pygm	Metabolism	-0.87	Down
Q9CQT1	Methylthioribose-1-phosphate isomerase GN=Mri1	Metabolism	-0.25	Down
P00920	Carbonic anhydrase 2 GN=Ca2	Metabolism		1U/1D
O89020	Afamin GN=Afm	Metabolism		1U/1D
O09131	Glutathione S-transferase omega-1 GN=Gsto1	Metabolism	1.22	Up
P97370	Sodium/potassium-transporting ATPase subunit beta-3 GN=Atp1b3	Metabolism	1.22	Up
P47739	Aldehyde dehydrogenase, dimeric ZDP-preferring GN=Aldh3a1	Metabolism	1.48	Up
Q9QYJ0	DnaJ homolog subfamily A member 2 GN=Dnaja2	Metabolism	2.00	Up
Q9R099	Transducin beta-like protein 2 GN=Tbl2	Unknown	-1.52	Down
Q00898	Alpha-1-antitrypsin 1-5 GN=Serpina1e	Unknown	-1.25	Down
Q9D7B7	Probable glutathione peroxidase 8 GN=Gpx8	Unknown		1U/2D
P00687	Alpha-amylase 1 GN=Amy1	Unknown		3U/2D
Q8CIT9	Suprabasin GN=Sbsn	Unknown	1.28	Up
Q9Z331	Keratin, type II cytoskeletal 6B GN=Krt6b	Unknown	1.30	Up
Q8CF02	Protein FAM25C GN=Fam25c	Unknown	1.81	Up

Table 2: Significantly enriched REACTOME pathways derived from CGSig dataset (120 proteins). Table is ordered from highest Entities Ratio to lowest. Entities Ratio is the number of proteins from Pathway Name/Total Number of Proteins for *Mus musculus* in REACTOME database. Entities pValue is hypothesis test of chances of the number of proteins found being within pathway compared to random significant pValue = enriched pathway. Accession numbers of proteins from CGSig which belong to a pathway, not an inclusive list of all proteins known within the pathway.

REACTOME Pathway identifier	Pathway name	Proteins Found in Pathway	Total Number of Proteins in Pathway	#Reactions found	#Reactions total	Entities Ratio	Entities pValue	Uniprot Accession of Proteins Found In Pathway
R-MMU-1266738	Developmental Biology	19	573	22	218	0.0520	0.00001468838	P97350; P04104; Q8CGR5; Q61414; Q3UV17; P15508; P97347; P28481; Q9R0Q6; Q61781; P43406; P08032; Q02257; Q9Z331; O35902; P55292; E9Q557; Q9JJZ2; A6BLY7
R-MMU-6798695	Neutrophil degranulation	14	532	8	10	0.0483	0.00202335301	P29699; P97350; P04104; P97449; Q61176; P43406; P16110; Q8VEH3; Q02257; Q9JM83; Q9EPB4; E9Q557; Q8R1Q8; P27005
R-MMU-6805567	Keratinization	13	191	14	26	0.0173	0.00000019904	P97350; P04104; Q8CGR5; Q61414; Q3UV17; P97347; Q61781; Q02257; Q9Z331; O35902; P55292; E9Q557; A6BLY7
R-MMU-397014	Muscle contraction	9	180	12	43	0.0163	0.00017018443	Q9JI91; Q8R429; Q9QZ47; P05977; P68134; P97457; P13412; P97370; P13542
R-MMU-5357801	Programmed Cell Death	5	151	6	155	0.0137	0.02528751686	P97350; O70456; P10637; O35902; E9Q557
R-MMU-381426	Regulation of Insulin-like Growth Factor (IGF) transport and uptake by Insulin-like Growth Factor Binding Proteins (IGFBPs)	4	123	1	6	0.0112	0.04619853375	P29699; Q61554; O55188; P63277
R-MMU-8957275	Post-translational protein phosphorylation	4	117	1	1	0.0106	0.03970547416	P29699; Q61554; O55188; P63277
R-MMU-109581	Apoptosis	5	110	6	110	0.0100	0.00733981442	P97350; O70456; P10637; O35902; E9Q557
R-MMU-1169410	Antiviral mechanism by IFN-stimulated genes	4	101	3	44	0.0092	0.02511274198	P63330; P10637; O55042; Q9JJZ2
R-MMU-6807878	COPI-mediated anterograde transport	4	100	6	12	0.0091	0.02433051178	P08032; P15508; Q9JJZ2; Q8R1Q8
R-MMU-1500931	Cell-Cell communication	4	100	5	56	0.0091	0.02433051178	Q91ZU6; P21570; Q02257; Q61781
R-MMU-6809371	Formation of the cornified envelope	13	98	7	19	0.0089	0.00000000008	P97350; P04104; Q8CGR5; Q61414; Q3UV17; P97347; Q61781; Q02257; Q9Z331; O35902; P55292; E9Q557; A6BLY7
R-MMU-373760	L1CAM interactions	4	76	3	24	0.0069	0.00988125906	P43406; P08032; P15508; Q9JJZ2
R-MMU-446728	Cell junction organization	4	76	5	40	0.0069	0.00988125906	Q91ZU6; P21570; Q02257; Q61781
R-MMU-9013106	RHOC GTPase cycle	3	75	2	6	0.0068	0.04930012225	P63024; Q02257; Q5FWK3
R-MMU-9013026	RHOB GTPase cycle	3	74	2	6	0.0067	0.04771882744	P63024; Q02257; Q5FWK3
R-MMU-9833482	PKR-mediated signaling	4	71	3	28	0.0064	0.00784286893	P63330; P10637; O55042; Q9JJZ2
R-MMU-3371497	HSP90 chaperone cycle for steroid hormone receptors (SHR) in the presence of ligand	3	71	4	22	0.0064	0.04312926881	Q9QYJ0; Q9JJZ2; Q8R1Q8
R-MMU-75105	Fatty acyl-CoA biosynthesis	3	70	4	20	0.0064	0.04165134733	P19096; Q5SWU9; O70503
R-MMU-9013406	RHOQ GTPase cycle	3	62	2	5	0.0056	0.03078079105	P63024; Q02257; Q5FWK3
R-MMU-3000178	ECM proteoglycans	4	52	7	14	0.0047	0.00264050200	O55188; P43406; P97399; P28481
R-MMU-75153	Apoptotic execution phase	4	50	4	53	0.0045	0.00229488049	P97350; P10637; O35902; E9Q557
R-MMU-375165	NCAM signaling for neurite out-growth	3	45	4	8	0.0041	0.01342809454	P08032; P15508; P28481
R-MMU-390522	Striated Muscle Contraction	6	39	4	4	0.0035	0.00000509269	Q9JI91; Q9QZ47; P05977; P68134; P13412; P13542
R-MMU-111465	Apoptotic cleavage of cellular proteins	4	38	4	38	0.0034	0.00084596405	P97350; P10637; O35902; E9Q557
R-MMU-1237044	Erythrocytes take up carbon dioxide and release oxygen	3	24	3	8	0.0022	0.00240137363	P00920; P13634; P04919
R-MMU-1480926	O2/CO2 exchange in erythrocytes	3	24	5	14	0.0022	0.00240137363	P00920; P13634; P04919
R-MMU-140875	Common Pathway of Fibrin Clot Formation	2	24	6	29	0.0022	0.02860143761	O88947; Q9Z126
R-MMU-1475029	Reversible hydration of carbon dioxide	2	17	2	8	0.0015	0.01507296362	P00920; P13634
R-MMU-1247673	Erythrocytes take up oxygen and release carbon dioxide	3	16	2	6	0.0015	0.00075788188	P00920; P13634; P04919
R-MMU-445095	Interaction between L1 and Ankyrins	2	12	1	1	0.0011	0.00778004526	P08032; P15508
R-MMU-351906	Apoptotic cleavage of cell adhesion proteins	3	11	3	10	0.0010	0.00025621707	P97350; O35902; E9Q557
R-MMU-446107	Type I hemidesmosome assembly	2	9	2	4	0.0008	0.00447020414	Q91ZU6; Q61781
R-MMU-5660668	CLEC7A/inflammasome pathway	1	4	2	3	0.0004	0.04264489669	Q9EPB4

Table 3: Welch's Two Sample T-Tests to test for significant difference in mean between treatment and control group crown area and skull length.

Crown area by Group			
	t = -1.1575	df = 47.474	p-value = 0.8736
95% Confidence Intervals	-0.02914971	Infinity	
Mean Control	1.021672mm^2		
Mean Treatment	1.033573mm^2		
Skull Length by Group			
	t = -86423	df = 41.17	p-value = 0.8038
95% Confidence Intervals	-0.5085681	Infinity	
Mean Control	19.02755mm		
Mean Treatment	19.20011mm		

Supplemental Figures:

Volcano Plots from Burroughs et al. (In Review) Tooth Proteomics

Low-dietary protein (10%) sample specimen over control (20% protein) sample specimen. Blue dots show adjusted p-value is ≤ 0.05. Labeled proteins refer to Table 1 in Burroughs et al. (In Review).

1: Treatment 1 Over Control 1

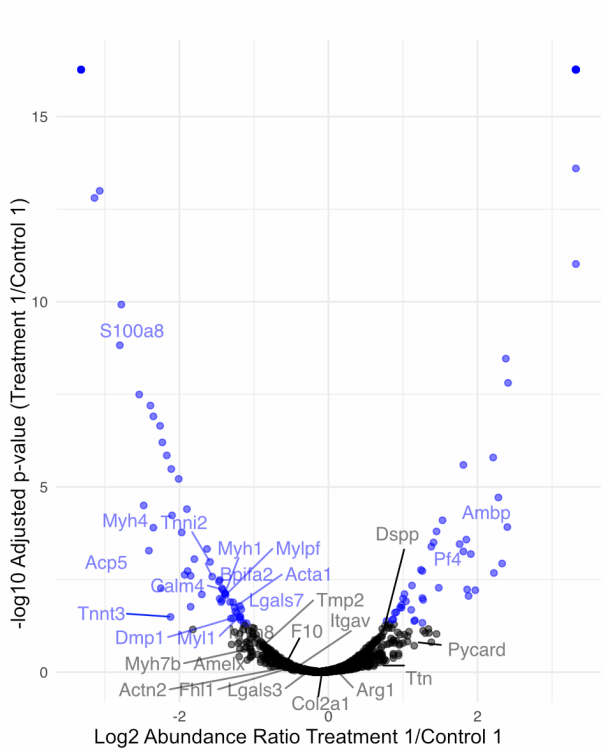

2: Treatment 1 over Control 2

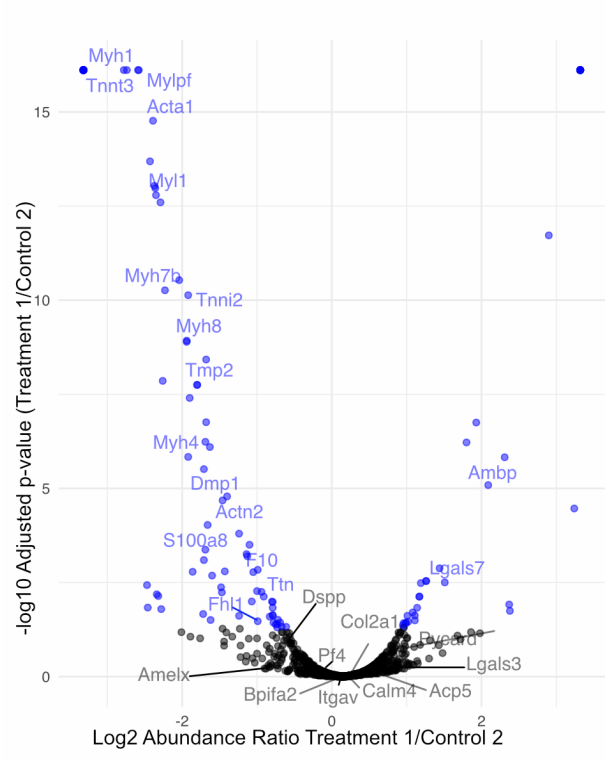

3: Treatment 2 over Control 2

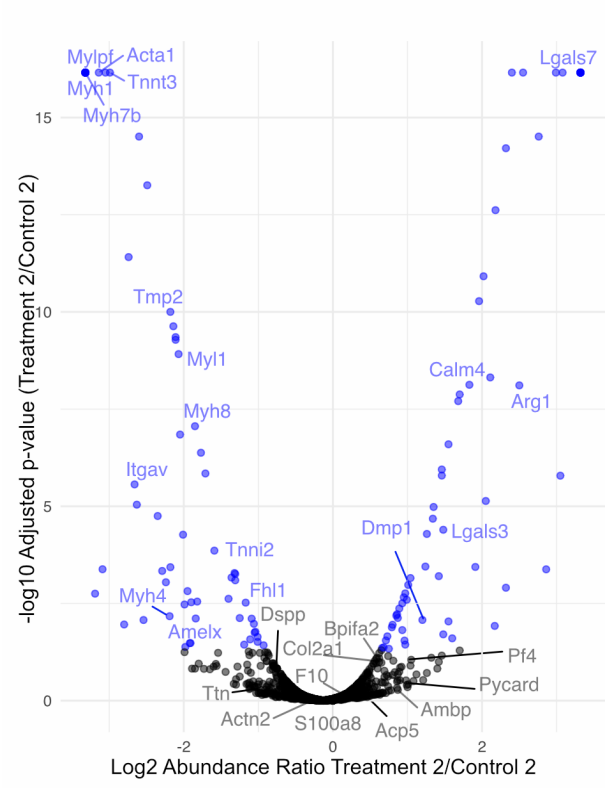

4: Treatment 3 over Control 3

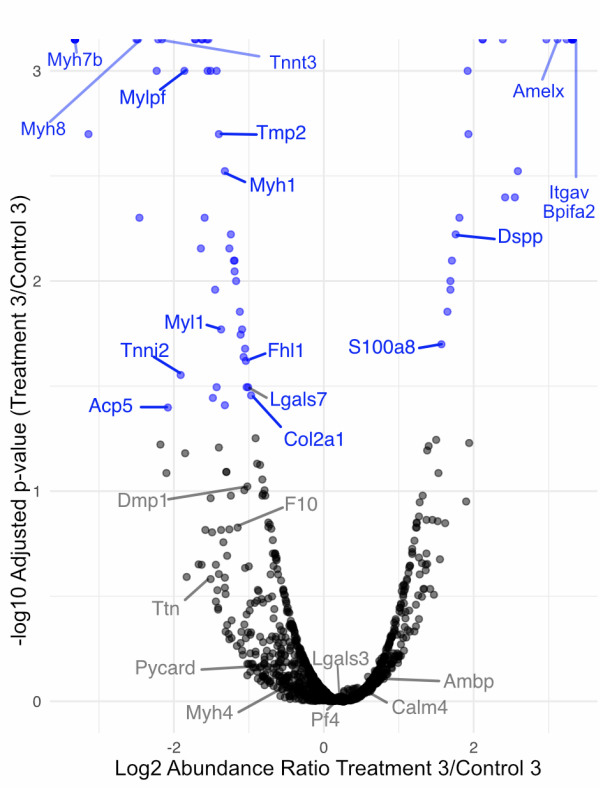

5: Treatment 4 over Control 3

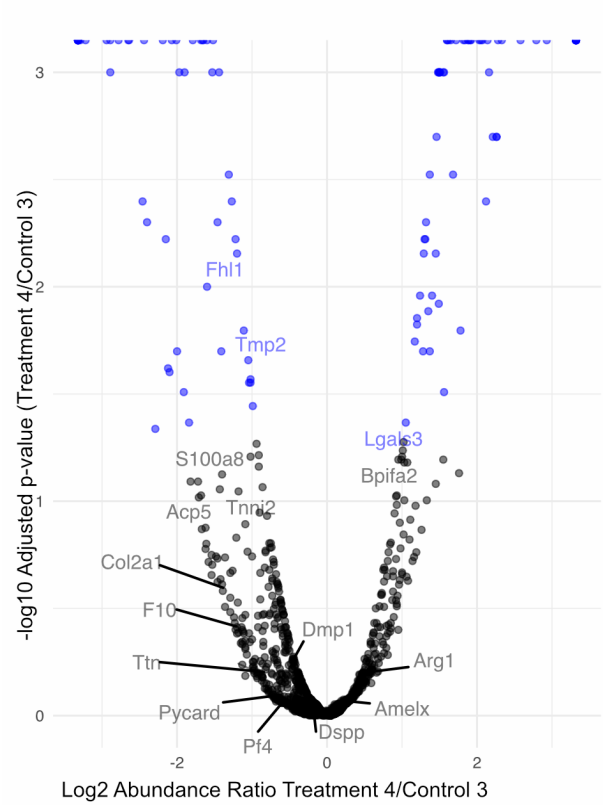
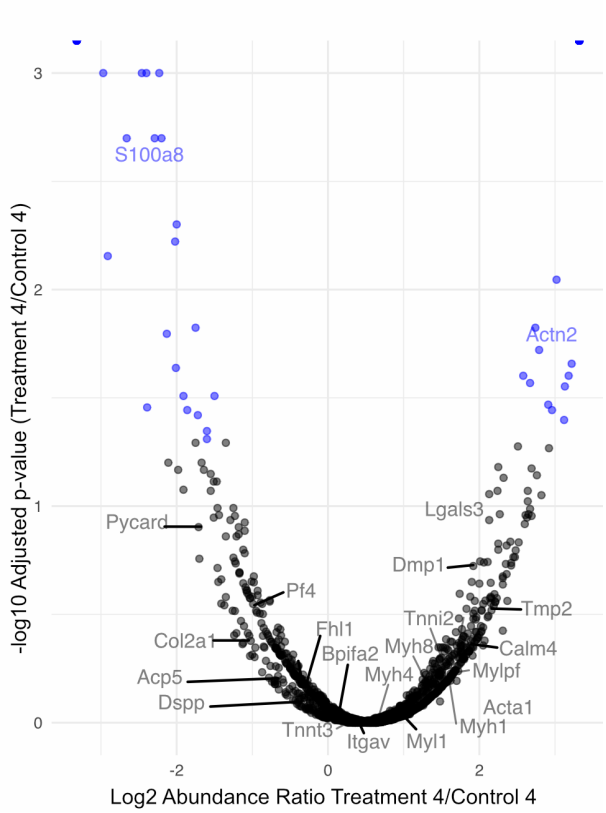
6: Treatment 4 over Control 4